
Energy and Density Analysis on the H₂ Molecule From the United Atom to Dissociation: The Σ, Π, Δ, Φ, and Γ Manifolds

GIORGINA CORONGIU,¹ ENRICO CLEMENTI²

¹*Università dell'Insubria, Dipartimento di Scienze Chimiche e Ambientali, Via Valleggio 11, I-22100 Como, Italy*

²*Via Carloni 38, I-22100 Como, Italy*

Received 16 March 2010; accepted 28 April 2010

Published online 20 August 2010 in Wiley Online Library (wileyonlinelibrary.com).

DOI 10.1002/qua.22831

ABSTRACT: We present 140 accurate potential energy curves, PECs, for the Σ, Π, Δ, Φ, and Γ manifolds for the H₂ molecule, mapping all the states with energy below the H₂⁺ ground state. The full configuration interaction, nonrelativistic Born–Oppenheimer computations are performed with large and optimized basis sets of Slater-type and spherical Gaussian functions; these new basis sets are somewhat larger than those used in recent published studies on the 60 Σ state PECs. The full CI computations are performed twice, with Hartree–Fock and with Heitler–London-type functions, allowing the identification of the ionic component in the total energy. The computed energies are within 10⁻⁵ hartree from the most accurate PECs in literature. We aim (a) at the evaluation of the PECs starting at very short and unexplored internuclear distances (0.01 bohrs) and ending at full dissociation, (b) at the systematic prediction of high excited state PECs dissociating as 1s + 4l and 1s + 5l, and (c) at the characterization of the evolution of the 140 PEC electronic densities from united atom to dissociation. With this work we fill a gap in today literature, which has dealt mainly with low excited states, generally excluding short internuclear distances. The electronic configuration at the united atom persists as dominant configuration well beyond the equilibrium separation, and it switches to that at dissociation often with energy patterns seemingly irregular, in particular when the values of the principal quantum number at dissociation and at the united atom differ by one or more unit. The Hund's singlet-triplet splitting, which propagates from the united atom to the molecule, is discussed. The singlet and triplet states are rather close in energy in the Π manifolds, and approach degeneracy in the Δ and Φ manifolds, to become fully degenerate in the Γ

Correspondence to: G. Corongiu; e-mail: corongiu@uninsubria.it

manifolds. Discussions on the correlation energy correction, adiabatic correction, spectroscopic constants and on general features of the H₂ excited states are presented. The H₂ molecule is a system, which—to be understood—needs consideration of both the very short internuclear distances in approaching the united atom and of the very high excited states below H₂⁺. © 2010 Wiley Periodicals, Inc. Int J Quantum Chem 111: 3517–3540, 2011

Key words: PECs for the Σ , Π , Δ , Φ , and Γ manifolds (gerade, ungerade, singlet, and triplets) in H₂; analysis of the electronic density; dissociation products; basis subset decomposition; radial distribution functions; full HF-CI; full HL-CI; Hund's multiplicity rule; correlation energy; adiabatic energy corrections

1. Introduction

The literature on computations of the H₂ molecule is very extended; it can be subdivided into three groups aimed (1) at specific physical-chemical properties of the molecule, (2) at proposing and testing algorithms for simulating these properties, and (3) at testing theoretical models proposed to provide a rigorous interpretation of the “chemical bond”. Our intent is to provide a more complete representation of the H₂ molecule by presenting new “computational data” particularly for excited states.

The solution of the Schrödinger equation has proved to be a difficult task, particularly in the time dependent formalism. Therefore, in the meantime we continue to make use of simpler, even semiempirical, approximations. As atomic spectroscopic data were fundamental for the development of the Bohr atomic theory, molecular spectroscopic data, in particular availability of potential energy curves, PECs, were and are basic to the development of molecular quantum mechanical models.

All models have theoretical validity boundaries leading to well known approximations, for example the Born–Oppenheimer and the nonrelativistic formulations; these approximations, however, do provide even today informative insights on molecules. A second type of boundaries for a model is the consequence of “historical” limitations on the available observations. There are still glaring limitations on our knowledge of H₂, such as absence of data for high excited states; these can be determined either from laboratory or—today—from computer simulations. A second glaring hole is the determination of the evolution of the H₂ PECs from short internuclear distances—around 1.0 bohrs—to 0.01 bohrs and from 0.01 to 0.0 bohrs;

the latter interval approaching the subatomic is not considered in this work.

In this article, we present computations of PECs for Π , Δ , Φ , and Γ high excited states complementing recent articles on the Σ manifolds [1–3], now recomputed with a somewhat larger basis set. For reasons of uniformity and completeness, we have also considered the low excited states, an opportunity to compare our results with the best data in literature [4–28]. Our work concerns the H₂ singlet and triplet states (gerade and un-gerade) dissociating into H(1s) + H(*nl*), with *n* from 1 to 5 and *l* from 0 to 4; a total of 140 states, precisely 60 Σ , 40 Π , 24 Δ , 12 Φ , and 4 Γ , crowding the energy region starting with the H₂ ground state and ending with the H₂⁺ ground state. In Table I, we anticipate a short characterization of the above 20 manifolds considered. The table gives the symmetry for each manifold (first column) and for the lowest and highest states in each manifold (second column) it reports the electronic configuration and the total energy at the united atom (third and forth columns), at dissociation (fifth and sixth columns) and the total energy at 2.0 bohrs (seventh column), a distance close to the equilibrium distance for 137 states out of 140. Only one energy value is reported for manifolds with degenerate singlet and triplet states.

Ideally, we should work with the time dependent Schrödinger equation, a particularly difficult task, which recently appears to be nearly in reach of a solution [29–33]. At the time of the first quantum chemical model by Heitler and London [34] the main target was the ground state of the H₂ molecule, since relatively little was known about the many H₂ excited states. We refer to the bibliography by McLean et al. [35] for a list of the many trials from the early quantum chemistry days to the year 1960, the start of computer simulations and of computational chemistry.

TABLE I
Low and high limits of the H₂ manifolds.

State manifold	State #	He conf.	E (u.a.)	Diss. conf.	E (diss.) 100 bohrs	E(eq.) 2.0 bohrs
$^1\Sigma_g^+$	1	$^1S(1s^1 1s^1)$	-2.90288	$1s^1 + 1s^1$	-1.00000	-1.17421 ^a
	16	$^1S(1s^1 8s^1)$	-2.00751	$1s^1 + 5s^1$	-0.52000	-0.59491
$^3\Sigma_g^+$	1	$^3S(1s^1 2s^1)$	-2.17521	$1s^1 + 2p^1$	-0.62500	-0.73708 ^b
	14	$^3D(1s^1 7d^1)$	-2.00961	$1s^1 + 5s^1$	-0.52000	-0.59842
$^1\Sigma_u^+$	1	$^1P(1s^1 2p^1)$	-2.12377	$1s^1 + 2p^1$	-0.62500	-0.75652 ^c
	15	$^1P(1s^1 8p^1)$	-2.00640	$1s^1 + 5s^1$	-0.52000	-0.58872
$^3\Sigma_u^+$	1	$^3P(1s^1 2p^1)$	-2.13313	$1s^1 + 1s^1$	-1.00000	-0.89706 ^d
	15	$^3H(1s^1 8h^1)$	-2.00713	$1s^1 + 5s^1$	-0.52000	-0.58881
$^1\Pi_g$	1	$^1D(1s^1 3d^1)$	-2.05562	$1s^1 + 2p^1$	-0.62500	-0.65951
	10	$^1D(1s^1 8d^1)$	-2.00619	$1s^1 + 5p^1$	-0.52000	-0.58090
$^3\Pi_g$	1	$^3D(1s^1 3d^1)$	-2.05563	$1s^1 + 2p^1$	-0.62500	-0.65956
	10	$^3D(1s^1 8d^1)$	-2.00619	$1s^1 + 5p^1$	-0.52000	-0.58090
$^1\Pi_u$	1	$^1P(1s^1 2p^1)$	-2.12377	$1s^1 + 2p^1$	-0.62500	-0.71817
	10	$^1F(1s^1 7f^1)$	-2.01015	$1s^1 + 5p^1$	-0.52000	-0.60359
$^3\Pi_u$	1	$^3P(1s^1 2p^1)$	-2.13313	$1s^1 + 2p^1$	-0.62500	-0.73746
	10	$^3F(1s^1 7f^1)$	-2.01015	$1s^1 + 5p^1$	-0.52000	-0.60511
$^1\Delta_g$	1	$^1D(1s^1 3d^1)$	-2.05562	$1s^1 + 3d^1$	-0.55556	-0.65753
	6	$^1D(1s^1 6d^1)$	-2.01378	$1s^1 + 5d^1$	-0.52000	-0.60605
$^3\Delta_g$	1	$^3D(1s^1 3d^1)$	-2.05563	$1s^1 + 3d^1$	-0.55556	-0.65759
	6	$^3D(1s^1 6d^1)$	-2.01379	$1s^1 + 5d^1$	-0.52000	-0.60610
$^1\Delta_u$	1	$^1F(1s^1 4f^1)$	-2.03125	$1s^1 + 3d^1$	-0.55556	-0.63393
	6	$^1H(1s^1 7h^1)$	-2.00985	$1s^1 + 5d^1$	-0.52000	-0.58826
$^3\Delta_u$	1	$^3F(1s^1 4f^1)$	-2.03125	$1s^1 + 3d^1$	-0.55556	-0.63393
	6	$^3H(1s^1 7h^1)$	-2.00985	$1s^1 + 5d^1$	-0.52000	-0.58826
$^{1,3}\Phi_g$	1	$^{1,3}G(1s^1 5g^1)$	-2.02000	$1s^1 + 4f^1$	-0.53125	-0.62261
	3	$^{1,3}G(1s^1 7g^1)$	-2.01005	$1s^1 + 5f^1$	-0.52000	-0.60266
$^{1,3}\Phi_u$	1	$^{1,3}F(1s^1 4g^1)$	-2.03125	$1s^1 + 4f^1$	-0.53125	-0.63372
	3	$^{1,3}H(1s^1 6h^1)$	-2.01382	$1s^1 + 5f^1$	-0.52000	-0.61377
$^{1,3}\Gamma_g$	1	$^{1,3}G(1s^1 5g^1)$	-2.02000	$1s^1 + 5g^1$	-0.520000	-0.62259
$^{1,3}\Gamma_u$	1	$^{1,3}H(1s^1 6h^1)$	-2.01382	$1s^1 + 5g^1$	-0.520000	-0.61374

^a R = 1.4 bohrs.

^b R = 1.9 bohrs.

^c R = 2.4 bohrs.

^d Not bound.

Studies on H₂ are as old as quantum chemistry: we present new potential energy curves, today available not only from experiments, such as in the old quantum chemistry days, but also from computations. We aim at the high excited states and at very short internuclear distances, presently unexplored; a more complete vision on the H₂ electronic states should lead to a better understanding of the molecule. Motivation for this work is not only the prediction of realistic potential energy curves and computation of the high excited states in H₂—not available in literature—but also the characterization of their electronic density evolution from the united atom to dissociation.

The large number of computations in literature dealing with the determination of the PECs for H₂ can be reduced to very few if one considers only the most accurate B-O energy computations, namely those by Kolos and co-workers [9–27], where James and Coolidge CI-type expansions [36, 37] with confocal elliptic coordinates are used. We, like other authors, see for example [28, 38–41], have explored more modern expansions and show that one can obtain accurate energies with simpler and more standard functions, such as Slater and Gaussian, rather unexplored at the time of the early computations by Kolos and co-workers.

The computations sample the internuclear separations from 0.01 to 100 bohrs. The deviations of

the computed energies from the most accurate computations in literature, 36 states in total [9–27], range from 4.3×10^{-6} to 4.5×10^{-5} hartree, a clear indication of the reliability of our computations.

In Section 2, we discuss computational details and we briefly report on the PECs of the Σ manifolds, recomputed with an improved basis set; the published analysis [1–3] on these states does not need re-elaboration. In Section 3, we present the PECs of the Π manifolds, in Section 4 those of the Δ , Φ , and Γ manifolds, in Section 5 relations of the Bohr model to H_2 PECs, in Sections 6 and 7 the PECs density analysis, in Section 8 comments on the triplet-singlet splitting (Hund's multiplicity rule), in Section 9 a discussion on the correlation energy correction, in Section 10 the decomposition of the total energy into kinetic, nuclear-electron and electron-electron components and a comment on the "origin of covalent binding," in Section 11 a short comment on the adiabatic correction and on computations of spectroscopic constants, and in Section 12 a few conclusions.

2. Computational Details and the PECs for the Σ Manifolds

Computationally, we use a well tested approximation of the Schrödinger equation, namely full configuration interaction B-O computations with extended and optimized basis sets. We consider both full MO-CI and full AO-CI (referred as Hartree-Fock CI, HF-CI, and Heitler-London CI, HL-CI). The two approaches yield the same energy for a given basis set, but the HL-CI technique is most convenient for the exploration of H^+H^- ionic states [1–3].

Accurate computations of the electronic states from He (united atom) to the H atoms (dissociation) require very extended basis sets capable also to describe helium, the united atom, from $He(1s1s)$ up to $He(1s^18l^1)$, and hydrogen from $H(1s)$ up to $H(5g)$ at dissociation. Two extended basis sets are used in this study: one is constructed with Slater-type functions, STF, the second with spherical Gaussian-type functions, GTF. The two optimized basis sets are nearly equivalent and the computations obtained with these two types of functions yield slightly different eigenvalues (and corresponding slightly different electronic densities) at a given internuclear separation,

thus, provide a useful numerical check and add flexibility to the interpretation of the electronic density. For additional discussion see Ref. [1]. With our nonorthogonal CI code [42] we obtain, for a given symmetry, all the needed roots, ground and excited states, directly by diagonalization, therefore, the state order is assigned unambiguously. Of the 117 internuclear separations considered for each PEC 15 are from 0.01 to 0.9 bohrs, 100 from 1.0 to 100 bohrs; computations at 1,000 and 10,000 bohrs are performed to accurately define the dissociation products.

The STF basis set centered on each one of the two hydrogen atoms is made by 10s, 10p, 7d, 6f, and 1g functions, yielding for the molecule 252 functions. The nearly equivalent GTF basis set is made by 18s, 11p, 12d, 8f, and 3g contracted to 13s, 11p, 9d, 6f, and 3g functions, yielding 320 contracted functions for the molecule. At the united atom the helium STF basis set is formed by 15s, 13p, 10d, 12f, 4g, and 3h yielding 257 STF functions. These basis sets are targeting mainly the high excited states of H_2 , the low ones being available [4–27].

The H_2 dissociation products are well represented by the STF basis set, which reproduces the hydrogenic energy with deviations of about 10^{-5} hartree. Also the helium atom excited state energies (singlet and triplet) with configuration from $(1s1s)$ up to $(1s8h)$ are nicely reproduced. The basis sets are available upon request to one of us (G. C.).

At dissociation the computations are carried out with the STF basis set augmented by hydrogenic functions; for each nl value an hydrogenic function is formed as a linear combination of Slater-type functions and used as a contracted Slater function; thus at dissociation our computations are exact in the nonrelativistic limit (see Table I). Note that preliminary experimentations with the hydrogenic basis set indicate that this set is optimal from dissociation to about 20 bohrs, without need of optimization.

All Σ state energies reported in this work have been recomputed with the above basis sets, since the basis sets used in previous articles [1–3] are somewhat smaller. In Figures 1 and 2 we report the PECs for the four Σ manifolds; in the figures we have included the ground state for the H_2 molecular ion (green color). The PECs from the new basis set for the states dissociating as $H(1s) + H(nl)$ with n from 1 to 4 have energies close to those given in Refs. [1–3]; the states dissociating

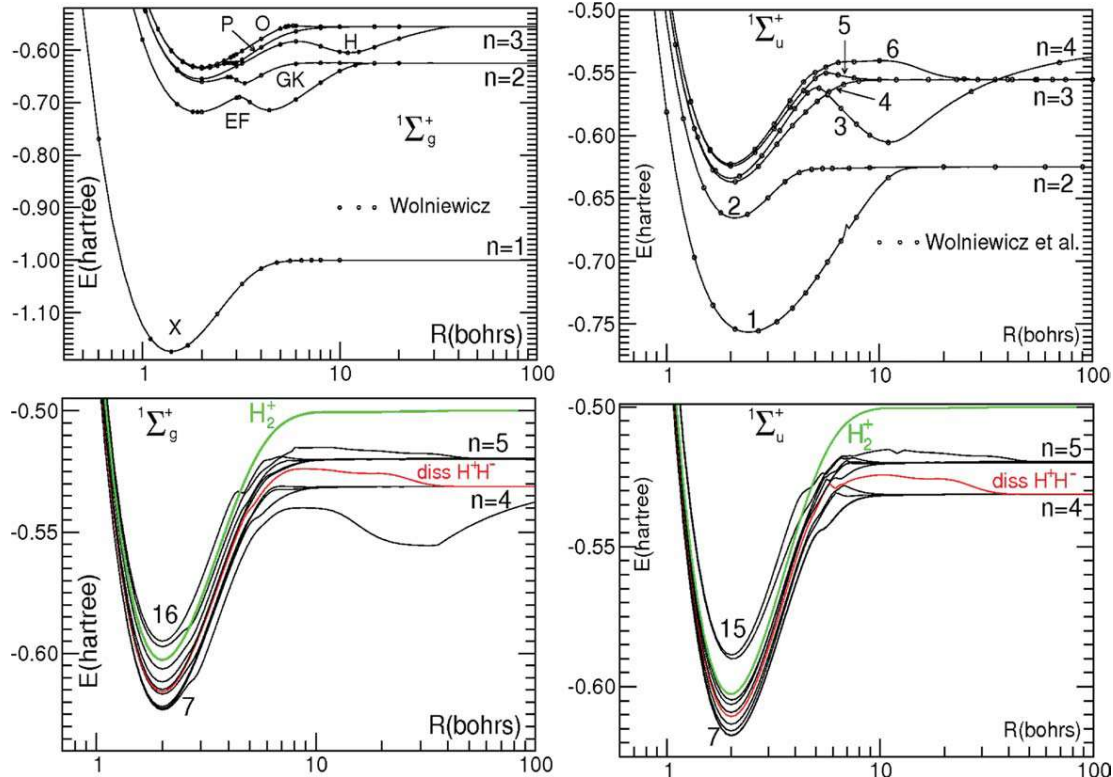


FIGURE 1. PECs for the singlet Σ manifolds from the extended basis set. Top: comparison of our computations (solid line) with selected values from Ref. [22–25] (dots). Bottom: our computations for high excited states. In red the PEC dissociating into H^+H^- . [Color figure can be viewed in the online issue, which is available at wileyonlinelibrary.com.]

with $n = 5$ have somewhat lower energies. The analyses on the electronic density from the new computations follow the one previously given [1–3]. Tabulation of the energies is available upon request to one of us (G.C.).

3. Computed PECS for the Π States

Experimentally [43], the first four $^1\Pi_u$ states, denoted C, D, D' and D'', have the following energies (in hartree) at the equilibrium distances (in bohrs): -0.718431 at 1.9517 , -0.655559 at 1.9857 , -0.632885 at 1.9993 and -0.622196 at 1.9710 , respectively. The first two $^1\Pi_g$ states, denoted I and R, have energies -0.658961 at 2.0207 bohrs and -0.633692 at 2.0031 bohrs, respectively. The first five $^3\Pi_u$ states, denoted $c(2p_{\pi})$, $d(3p_{\pi})$, $k(4p_{\pi})$, $n(5p_{\pi})$, and $u(6p_{\pi})$, have the following energies (in hartree) and equilibrium distances (in bohrs): -0.737802 at 1.9608 , -0.660973 at 1.9835 , -0.635158 at 1.9931 , -0.623372 at 1.9994 and

-0.611821 at $[2.0201]$, respectively. The first $^3\Pi_g$ state, denoted $i(3d_{\pi})$, has energy (-0.659007) at 2.0220 bohrs and the second state, denoted $r(4d_{\pi})$, has an energy of -0.634030 hartree.

In this article, rather than using the above spectroscopic notation [43], we adopt the numerical designation 1, 2, ..., 10 to denote the different excited states.

The $^1\Pi_u$ and the $^1\Pi_g$ excited states have been often studied in the past and even recently [9–15]; the most accurate PECs for the first four $^1\Pi_u$ states are those reported by Wolniewicz and Staszewska [15], somewhat more accurate than those by Spielfiedel [41]. The most accurate PECs for the $^1\Pi_g$ excited states are those reported by Wolniewicz [11] for the first two states, with energies slightly lower than those for three $^1\Pi_g$ states computed by Spielfiedel [41]. The most accurate PECs for the three lowest $^3\Pi_u$ excited states are those reported by Staszewska and Wolniewicz [16] and for the $^3\Pi_g$ manifold those in Ref. [16] for the states 1 and 2 and in Ref. [17] for state 3.

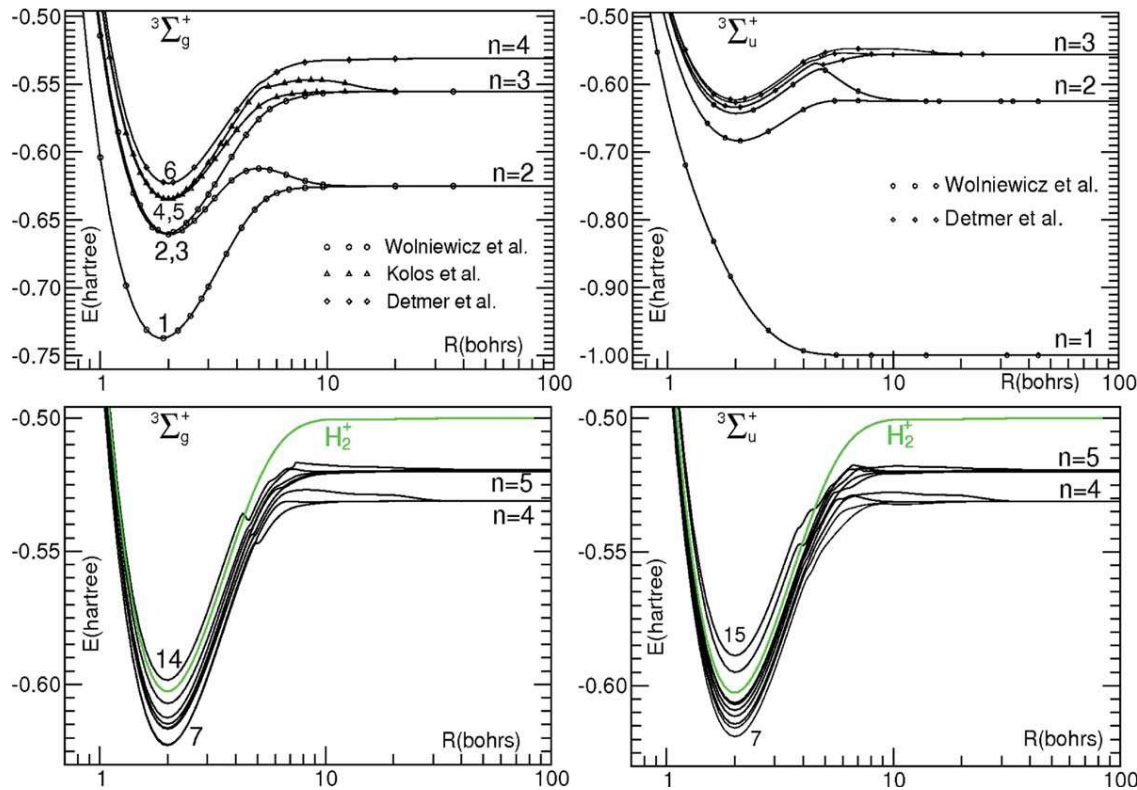


FIGURE 2. PECs for the triplet Σ manifolds from the extended basis set. Top: comparison of our computations (solid line) with selected values from Ref. [16] (dots), from Ref. [27] (triangles), from Ref. [41] (diamonds). Bottom: computation for high excited states. [Color figure can be viewed in the online issue, which is available at wileyonlinelibrary.com.]

The dissociation products for the Π manifolds are two H atoms, one, $H[{}^2S(1s^1)]$, is present in all state dissociation products, whereas the second for the states 1 to 10 is $H[{}^2P(2p^1)]$, $H[{}^2D(3d^1)]$, $H[{}^2P(3p^1)]$, $H[{}^2F(4f^1)]$, $H[{}^2D(4d^1)]$, $H[{}^2P(4p^1)]$, $H[{}^2G(5g^1)]$, $H[{}^2F(5f^1)]$, $H[{}^2D(5d^1)]$, and $H[{}^2P(5p^1)]$, respectively.

For the ${}^1\Pi_u$ manifold, starting with state 1 and proceeding to state 10, the states at the united atom are $He[{}^1P(1s^12p^1)]$, $He[{}^1P(1s^13p^1)]$, $He[{}^1F(1s^14f^1)]$, $He[{}^1P(1s^14p^1)]$, $He[{}^1F(1s^15f^1)]$, $He[{}^1P(1s^15p^1)]$, $He[{}^1H(1s^16h^1)]$, $He[{}^1F(1s^16f^1)]$, $He[{}^1P(1s^16p^1)]$, $He[{}^1F(1s^17f^1)]$; for the ${}^1\Pi_g$ manifold the states are $He[{}^1D(1s^13d^1)]$, $He[{}^1D(1s^14d^1)]$, $He[{}^1G(1s^15g^1)]$, $He[{}^1D(1s^15d^1)]$, $He[{}^1G(1s^16g^1)]$, $He[{}^1D(1s^16d^1)]$, $He[{}^1G(1s^17g^1)]$, $He[{}^1D(1s^17d^1)]$, $He[{}^1G(1s^18g^1)]$, and $He[{}^1D(1s^18d^1)]$.

The 10 ${}^3\Pi_u$ states merge into $He[{}^3P(1s^12p^1)]$, $He[{}^3P(1s^13p^1)]$, $He[{}^3P(1s^14p^1)]$, $He[{}^3F(1s^14f^1)]$, $He[{}^3P(1s^15p^1)]$, $He[{}^3F(1s^15f^1)]$, $He[{}^3P(1s^16p^1)]$, $He[{}^3H(1s^16h^1)]$, $He[{}^3F(1s^16f^1)]$, $He[{}^3F(1s^17f^1)]$, and the 10 ${}^3\Pi_g$ states into $He[{}^3D(1s^13d^1)]$, $He[{}^3D(1s^14d^1)]$, $He[{}^3D(1s^15d^1)]$, $He[{}^3G(1s^15g^1)]$, $He[{}^3G(1s^16g^1)]$, $He[{}^3G(1s^17g^1)]$, $He[{}^3D(1s^18d^1)]$.

[${}^3D(1s^16d^1)$], $He[{}^3G(1s^17g^1)]$, $He[{}^3D(1s^17d^1)]$, $He[{}^3G(1s^18g^1)]$ and $He[{}^3D(1s^18d^1)]$. The helium high excited states, for a given n are very close in energy, nearly degenerate.

In Figure 3 we report the computed PECs, those from $R = 0.7$ to $R = 20$ bohrs, for the first 10 ${}^1\Pi_u$ states (top left inset), ${}^1\Pi_g$ states (top right inset), ${}^3\Pi_u$ (bottom left inset) and ${}^3\Pi_g$ (bottom right inset). In the figure the small circles selectively sample the energies from Refs. [11, 15–17] and the triangles from Ref. [41]. In each inset, we report in addition the PEC for the ground state of H_2^+ (green color). Recall that the computed energy of the H_2^+ ion for the ${}^2\Sigma_g^+(1\sigma_g)$ and ${}^2\Sigma_u^+(1\sigma_u)$ states (obtained with the same basis set used in this work) at 2.0 bohrs, are -0.602633 and -0.167533 hartree, respectively; these values differ by 1.5×10^{-6} hartree from the best results in Ref. [44].

In tabulations, available upon request to one of us (G.C.), we provide the computed energies for the Σ , Π , Δ , Φ , and Γ manifolds.

Our computed energies compare well with the accurate values of Wolniewicz et al. [11, 15–17] and

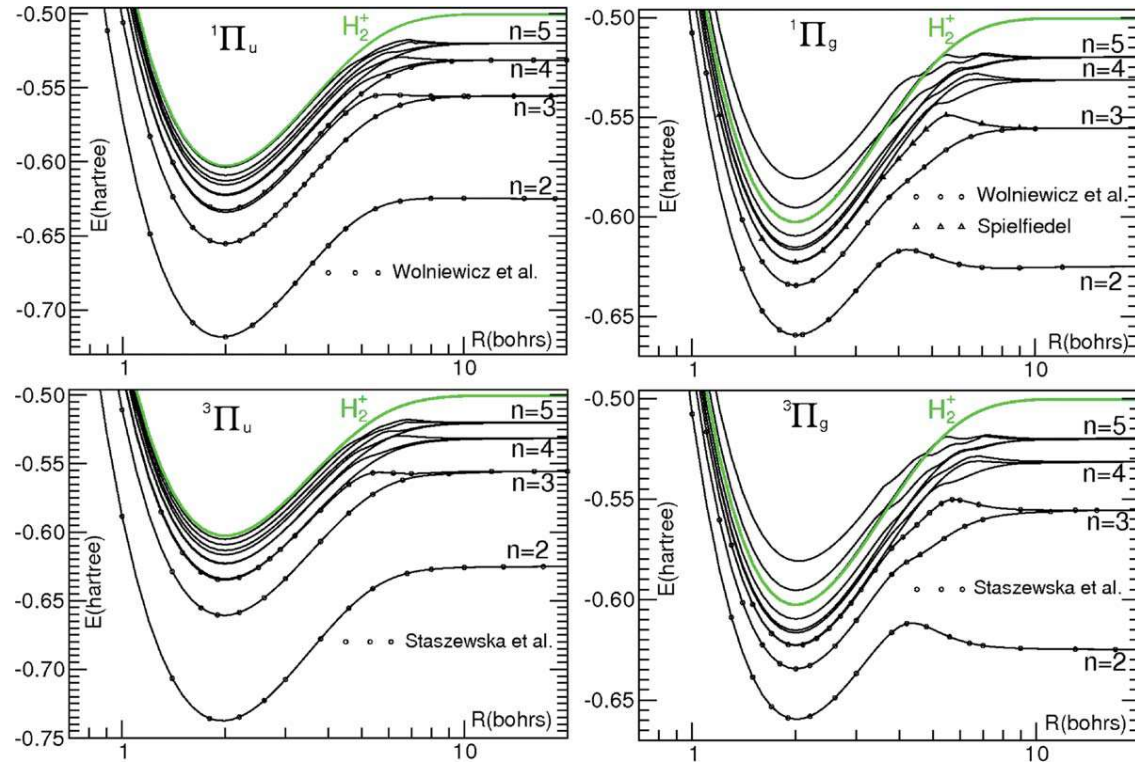


FIGURE 3. Computed PECs from $R = 0.7$ to $R = 20$ bohrs for the excited state manifolds $^1\Pi_u$ (top left, circles from Ref. [15]), $^1\Pi_g$ (top right, circles from Ref. [11], triangles from Ref. [41]), $^3\Pi_u$ (bottom left, circles from Ref. [16]), $^3\Pi_g$ (bottom right, circles from Refs. [16, 17]). [Color figure can be viewed in the online issue, which is available at wileyonlinelibrary.com.]

Spielfiedel [41]. For the $^1\Pi_u$ manifold the average deviations (in hartree) from Ref. [15] for states 1–4 are: 4.5×10^{-5} , 2.0×10^{-5} , 1.4×10^{-5} and 1.7×10^{-5} . For the $^1\Pi_g$ manifold the average deviations (in hartree) from Ref. [11] for states 1 and 2 are: 7.7×10^{-6} , 7.8×10^{-6} ; for state 3 comparing our energies are somewhat lower than those in Ref. [41]. For the $^3\Pi_u$ manifold the average deviations (in hartree) from Ref. [16] for states 1 to 3 are: 1.6×10^{-5} , 9.4×10^{-6} , 1.3×10^{-5} . For the $^3\Pi_g$ states 1–3 the average deviations (in hartree) from Refs. 16 and 17 are: 7.7×10^{-6} , 6.7×10^{-6} , and 4.3×10^{-6} .

In conclusion, the computed PECs reproduce nicely the best computed energies in the literature, and therefore, are reliable for the density analysis presented in this work. Further, we note that the largest energy deviations are for the low states. This is due to our targeting this study to the high excited states, because for the low ones accurate data are already available.

For very short internuclear distances, from $R = 0.01$ to $R = 0.9$ bohrs, we show in Figure 4 the full CI computed results. The PECs in these fig-

ures correspond to electronic rather than total energies (requiring a smaller energy range compared to the one needed in showing the corresponding total energies). In each figure, the PECs merge into the corresponding helium excited state energies smoothly and not linearly, as noted in Refs. [1–3].

From $R = 0.01$ to 0.07 bohrs the PECs are obtained from computations with the helium STF basis set centered midway between the two hydrogen nuclei. For the internuclear distances from 0.08 to 0.9 bohrs, we report CI computed energies obtained with GTF centered on the two H atoms. In the figures, we have indicated with a short vertical bar the internuclear separation at 0.08 bohrs. For some PECs, the small energy discontinuity between 0.07 and 0.08 bohrs is because of the different computational techniques with different basis sets. As one can appreciate from Figure 4, the change of computational technique at very short distances does not invalidate the overall conclusion: the PECs smoothly, and not linearly, merge into the united atom.

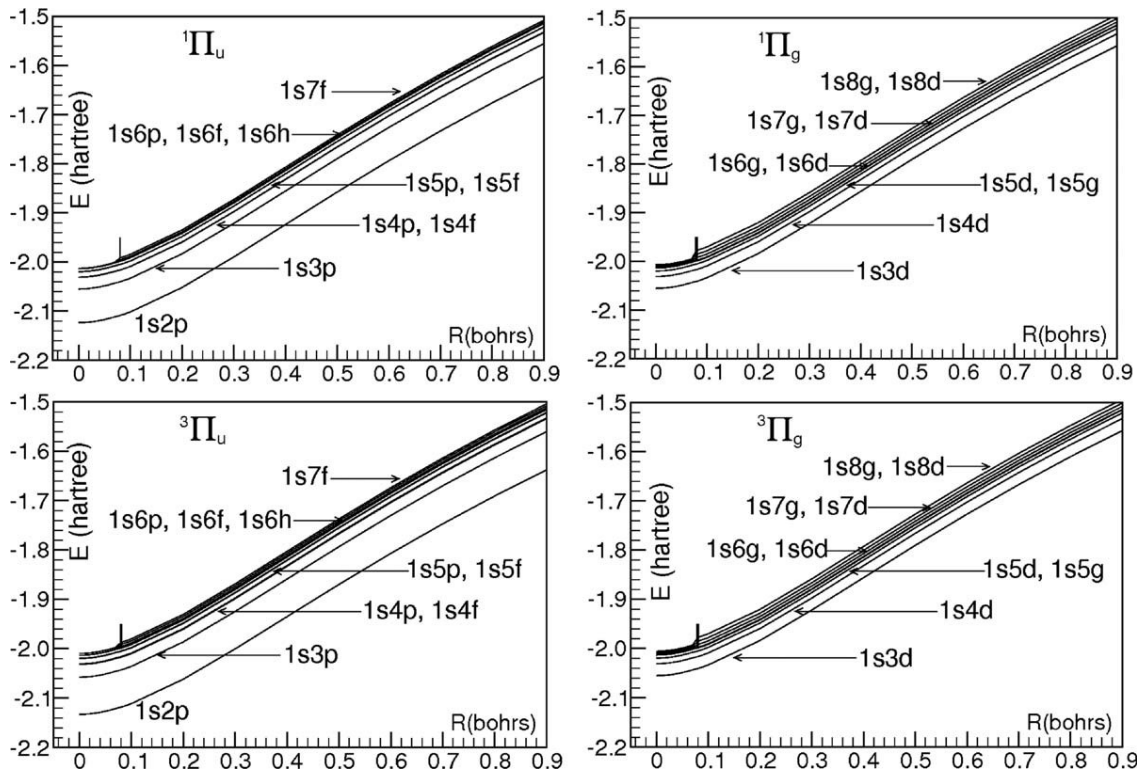


FIGURE 4. PECs at short internuclear distances, from $R = 0.01$ to $R = 0.9$ bohrs, for the manifolds $^1\Pi_u$ (top left), $^1\Pi_g$ (top right), $^3\Pi_u$ (bottom left), and $^3\Pi_g$ (bottom right).

We recall that the computations with full CI of Heitler–London orbitals allows to quantitatively evaluate the ionic energy percentage [1–3] linking the covalent and the ionic components to the total energy for a given state at a defined internuclear separation. From our computations we conclude that in the Π states the ionic energy percentage is essentially negligible. For the $^1\Pi_u$ manifold there is a small effect for states 3, 5, and 6 and for the $^1\Pi_g$ manifold for states 1 and 3 in the region between 4 and 6 bohrs.

Both the first $^1\Pi_g$ and $^3\Pi_u$ states approach dissociation from lower energies, whereas the first $^1\Pi_u$ and $^3\Pi_g$ states approach dissociation from higher energies. In addition, the first $^1\Pi_u$ state shows a van der Waals maximum in the region 9–9.5 bohrs, whereas the first $^1\Pi_g$ state shows a minimum around 8 bohrs. These van der Waals features were predicted by Mulliken [8] on the base of long-range first-order interaction theory.

Inspection of the PECs in Figures 3 and 4 can lead to a rough guess of the PEC electronic configurations. Indeed, for all states we expect that near dissociation the density is characterized by the configura-

tion $(1s^1nl^1)$ with n defined by the corresponding dissociation products. At shorter internuclear separations—from full dissociation to about 10 bohrs—we expect from previous studies [1–3] that only the l values undergo switches within their set of values (from $l = n-1$ to $l = 1$). Furthermore, we expect the occurrence of heavy configuration mixing due to the closeness and the crossing of states at R values in the interval 10 to 5 bohrs for the Π_u manifolds and 10 to 4 bohrs for the Π_g manifolds, the “ n matching” region. For a given PEC the mixing is expected to be stronger the higher the n value of the dissociation products, where near degeneracy is reached. The over all effect is a stronger and stronger state-to-state interaction, with increased probability and near degeneracy or state crossing. In these conditions the state is no longer characterized by a *main single* configuration but by a *combination* of configurations. Finally, on the base of previous studies [1–3], we expect the dominant configuration to be the one of the united atom from 0 to about 3–4 bohrs.

The states in the Π_g manifolds, with the electrons in “antibonding orbitals”, depart from the united atom configuration after equilibrium at about 4

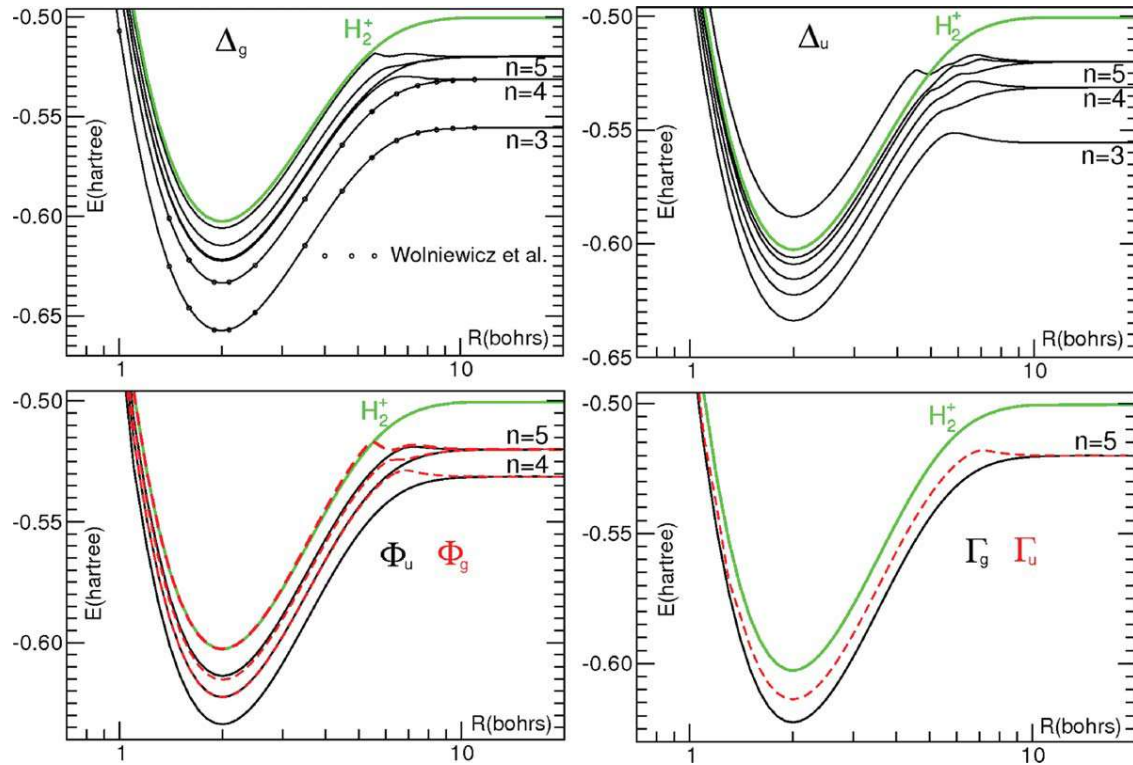


FIGURE 5. Computed PECs from $R = 0.7$ to $R = 20$ bohrs for the excited state manifolds Δ_g (top left, dots from Ref. [20]) and Δ_u (top right), Φ (bottom left) and Γ (bottom right). [Color figure can be viewed in the online issue, which is available at wileyonlinelibrary.com.]

bohrs, a somewhat shorter internuclear distance than for the Π_u manifolds, characterized by the electrons in “bonding orbitals”. Note that in high excited states, the n value in the dominant nl configuration at the united atom is higher than the n value in the dominant nl configuration at dissociation; in such cases in switching from the united atom to the dissociation configuration there is a concomitant “de-excitation” process, an “energy lowering” (with a lower n value). Clearly, the higher the value of n at the united atom, the larger the energy stabilization, with the likely presence of “irregularities” in the PECs approaching dissociation.

the value is not given [43]. The corresponding equilibrium energies (in hartree) are given as (-0.657102) , $[(-0.628201)]$, (-0.657180) , and -0.632839 , respectively. As for the Π states, rather than the spectroscopic notation, we adopt the numerical designation $1, 2, \dots, 6$ to denote the different excited states. There are no experimental spectroscopic data for the Φ and Γ states.

These (somewhat uncertain) laboratory data have been computationally analyzed mainly for the low Δ states [19, 20, 41]. The PEC for the first two ${}^1\Delta_g$ states—from small distances to about 10 bohrs—have been accurately reported first by Wolniewicz [19] and later improved by the same author [20]; for the first ${}^1\Delta_u$ state there is the PEC computation by Spielfiedel [41]. There are no computations for the Φ and Γ states.

The dissociation products of the Δ , Φ , and Γ manifolds have the configuration $\text{H}[{}^2S(1s^1)]$ and $\text{H}[{}^2X(nl^1)]$; for the Δ states $3 \leq n \leq 5$; for the Φ states $4 \leq n \leq 5$ and for the Γ states $n = 5$. The electronic configurations of the dissociation products and of the united atom for the first and the last states are given in Table I.

4. Computed PECS for the Δ , Φ , and Γ Manifolds

Experimentally [43], two excited states are reported for each one of the ${}^1\Delta_g$ and ${}^3\Delta_g$ manifolds J, S and j and s , respectively. The equilibrium distances (in bohrs) for the J, S , and j states are 1.9929, [(2.0371)], and 1.9927; for the s state

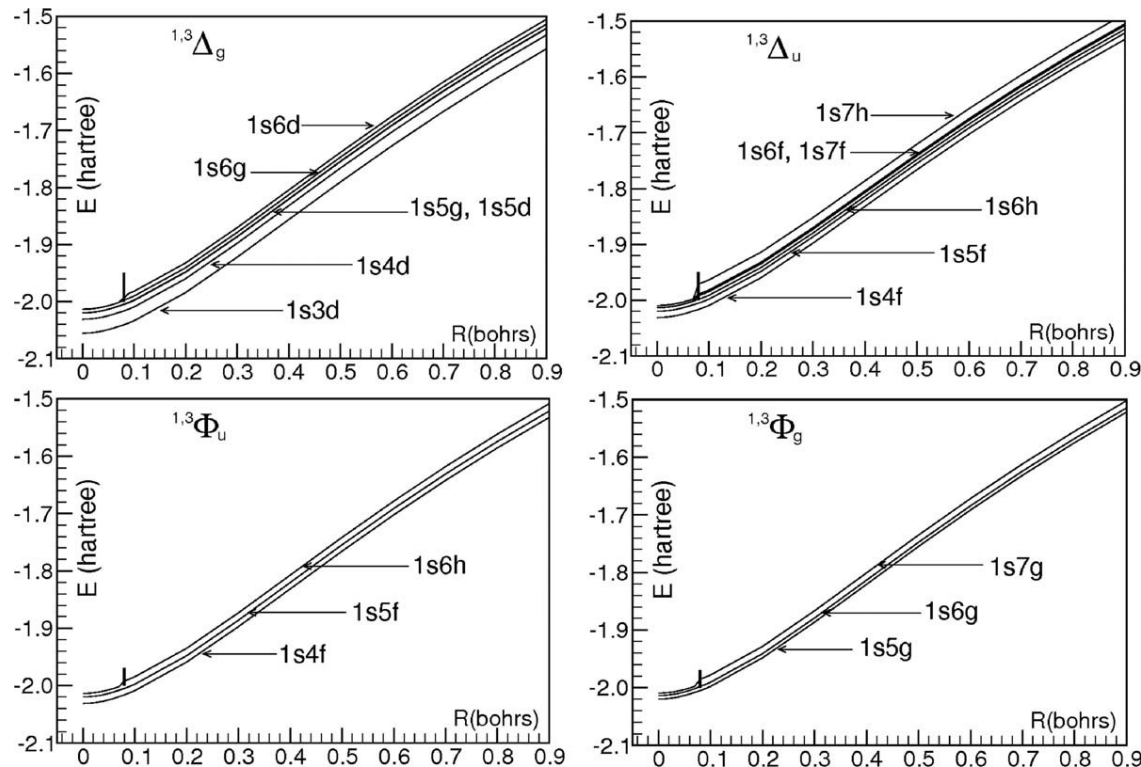


FIGURE 6. PECs at short internuclear distances, from $R = 0.01$ to $R = 0.9$ bohrs, for the ${}^1,{}^3\Delta_g$, ${}^1,{}^3\Delta_u$, ${}^1,{}^3\Phi_g$, and ${}^1,{}^3\Phi_u$ states.

In the top left inset of Figure 5, we report the computed PECs for the ${}^1,{}^3\Delta_g$ states 1–6 (the small circles represent a selected sample of energies from Ref. [20]) and in the top right inset the PECs for the ${}^1,{}^3\Delta_u$ states 1–6. In Figure 5 we report also the PECs for the Φ and for the Γ states (bottom insets). In this figure, we have reported the energies of singlet states only since the triplet-singlet splitting is exceedingly small. As expected the Δ and Φ states dissociating with $n = 5$ are irregular in the n matching region between 5 and 10 bohrs.

Our computed energies compare well with the accurate values by Wolniewicz [20] and Spielfiedel [41]. For the states 1 and 2 of the ${}^1\Delta_g$ manifold, the average deviations (in hartree) from Ref. [20] are 4.4×10^{-5} and 1.9×10^{-5} , respectively. The same deviations are found for the ${}^3\Delta_u$ states, as the triplet-singlet splitting is very small. For the first ${}^1\Delta_u$ state the average deviation (in hartree) from Ref. [41] is 2.0×10^{-5} in our favor.

For very short internuclear distances, from $R = 0.01$ to $R = 0.9$ bohrs, we report in Figure 6 our computed PECs. In each inset the PECs merge into the corresponding helium excited state energies smoothly and not linearly.

5. From the United Atom to Dissociation Products

Physically, the H_2 molecule is that system which starts as He and ends as two H atoms. The energy pattern of the PECs in H_2 is dominated by atomic configurations: the $(1s n)$ at the united atom, which persists well beyond equilibrium separation, and the $1s$ and $n'l'$ of the two H atoms at dissociation. As a consequence of the few particles in the molecule the energy pattern of the H_2 PECs can be rationalized with simpler models than the full CI adopted in our computations.

Let us consider the energies of initial and final atomic states. We denote with n_1 and n_2 the principal quantum numbers of the two electrons in He and n'_1 and n'_2 those of the two electrons at the dissociation products of H_2 . For the states in discussion $n_1 = n'_1 = 1$, and, in general, $n_2 \neq n'_2$; the latter differentiation is most important.

In the Bohr model, the state energy for hydrogenic systems is proportional to the inverse of principal quantum number squared

$$E = -Z^2/2n^2 \quad (1)$$

For the He atom, the n dependency can be evidenced by writing [45]

$$E = -[Z_{\text{eff}}^2/n_1^2 + Z_{\text{eff}}^2/n_2^2] + \text{higher terms.} \quad (2)$$

where the charge Z seen from an electron is partially screened and appears as an effective charge, Z_{eff} (for screening constants rules see [46, 47]); note that a better approximation is obtained by replacing the Z_{eff} with two different values, $Z_{1,\text{eff}} \neq Z_{2,\text{eff}}$, one for each electron.

In Eqs. 1 and 2, the emphasis is on the electronic energy dependency from the corresponding principal quantum numbers; Eq. (2) reminds us on the propagation process starting with n_1 , n_2 and Z_{eff} (or $Z_{1,\text{eff}}$ and $Z_{2,\text{eff}}$) at the united atom and ending with n'_1 , n'_2 and $Z = 1$ at dissociation. Stated differently, the energy path of any H_2 state is that described at the start with $Z_{1,\text{eff}}$, $Z_{2,\text{eff}}$, $n_1 = 1$ and a given n_2 and at the end by $Z = 1$ with $n'_1 = 1$ and a given n'_2 .

For given n'_2 and n_2 , from Eqs. 1 and 2 we see that the atomic excitation energy increases faster at the united atom than at dissociation; thus a PEC with $n_2 \neq n'_2$ experiences for $n_2 \geq n'_2$ a variation in the principal quantum number, which—as we shall see—can lead to “irregularities” in the PEC.

By considering the states from $\text{He}(1s^2)$ to $\text{He}(1s^15l^1)$ (both singlet and triplet states, see the atomic energy level tables [48] or the data in Table I), we realize that these states are not sufficient to lead to the first 140 states in H_2 (those which dissociate from $n = 1$ to $n = 5$, namely from $\text{H}(1s^1) + \text{H}(1s^1)$ to $\text{H}(1s^1) + \text{H}(5l^1)$). Indeed, it is apparent that we must include in the He set additional states, up to $1s^18l^1$. Thus, the energy pattern of several excited states of H_2 will be characterized by a lowering of the principal quantum number in the evolution from united atom to dissociation.

Let us consider now the first 140 states in the H_2 molecule (see Table I) keeping in mind that the nl value at dissociation often is different from the nl value at the united atom. The n value lowering is obtained via repeated state crossing occurring particularly in the internuclear distance region from 4–6 to about 10 bohrs (or more), where the dissociation process begins. Further, from Eqs. 1 and 2, we see that the higher the values of n the closer the state energies not only at the united atom but also at intermediate internuclear distances and at dissociation. Thus, the expectation of closer and closer state energies, with

concomitant stronger and stronger state to state interaction and eventual state crossing.

In conclusion, we have shown that the Bohr model at the united atom and at dissociation implies important features for the H_2 excited states.

6. Analysis of the PEC: Molecular Probability Distribution

In the following sections, we characterize the evolution of the PEC electronic density from the united atom to dissociation. Each PEC at any internuclear separation has a characteristic electronic density, originated either by a single main configuration ($1s^1nl^1$) or a mixture of configurations. We use two approaches, one “designated molecular probability distribution” and the other “basis subset decomposition.”

The first technique considers for each PEC, at selected internuclear distances, the molecular radial distribution function defined in Refs. [1] and [2] and denoted “state- $D_{R,nl}(r)$,” where state designates a specific state (1, 2,...), R is the specific internuclear separation considered, and nl is a short-hand notation to designate the configuration $1snl$ or a mixing of configurations.

The molecular state- $D_{R,nl}(r)$ is the equivalent of the familiar atomic radial distribution function $D_{nl}(r)$ [49]. Consider two hydrogen atoms, both positioned on the z -axis at a distance R , one atom at $z = -R$ and the second at $z = 0$. For a given state wave function, the state- $D_{R,nl}(r)$ distributions are computed on an axis departing from the origin and ending at r values where the state electronic density vanishes. For a given manifold, the axis is selected for the best representation for different values of the l in the $1snl$ configuration. Generally, we compute the state- $D_{R,nl}(r)$ along two different axis, obtaining two different intensities, mutually consistent. The graphical representation of a molecular radial distribution function is compared (considering the number, intensity, position of the nodes and the overall shape) to two sets of “reference $D_{R,nl}(r)$,” those of the He and H atoms. The “state- $D_{R,nl}(r)$ ” are computed for each state at several (generally seventeen) internuclear distances; their plots allow identification by inspection of the electronic density at a given R . The molecular “state- $D_{R,nl}(r)$ ”

TABLE II

$^1\Pi_u$ manifold: configurations $1snl$ for states 1 to 10 at different internuclear separations: nl from “state- $D_{nl}(r)$ ” analyses, (nl) from basis subset analysis (see text).

#	0.1	0.5	1.8	2.0	2.2	3.0	4.0	5.0	6.0	8.0	10.0	15.0	30.0	100
1	2p	2p	2p	2p	2p									
2	3p	3d	3d	3d	3d									
3	4f	3d	3d	3d	3p	3p	3p							
4	4p	4d	4d	4f	4f	4f								
5	5f	4d	4f	4f	4d	4d	4d							
6	5p	(4l/5d)	(4l/5d)	4p	4p	4p								
7	6p	5p	5f	(4l/5d)	(4l/5d)	(4l/5d)	5g	5g						
8	6f	6d	6p	(5p/5d)	(5p/5d)	5f	5f	5f						
9	6h	6h	6h	6h	6h	7f	7f	7p	6d	(5f/5g)	5f	5d	5d	5d
10	7p	7f	7p	(4l/5l)	(4l/5l)	(5l)	5p	5p						

function for a given nl is somewhat different at different internuclear separations, both in shape and in the relative intensity between nodes, because the electronic promotion and polarization functions contribute to the wave function differently at different R values.

The analyses for each manifold is condensed in Tables II–V, reporting the configurations state by state at several internuclear separations. The identification nl given in the tables refers to the *main* configuration. When—at a given internuclear separation—two or more states either cross or nearly cross or are strongly interacting with other nearby states then the identification of the positions and number of minima and maxima in the $D_{nl}(r)$ might become fuzzy. Ionic structures can participate to the density, increasing fuzziness. In these cases, we make use of additional criteria to identify the configurations, such as the basis subset decomposition analysis (see next Section); in such

cases the identification of the configuration is reported in the Tables within parentheses, (nl).

In Figure 7 we provide, for the first five $^1\Pi_u$ states, examples of the molecular radial distribution analysis. In the left top inset, we present the radial distribution functions of the united atom, namely the $D_{nl}(r)$ at $R = 0$ corresponding to the first five $^1\Pi_u$ states (see Section 3). In the top right inset, we present the superimposed radial distribution functions of $\text{H}[^2\text{S}(1s^1)]$ and of $\text{H}[^2\Gamma(nl^1)]$ at dissociation, $R = \infty$. These $D_{nl}(r)$ distributions constitute our “reference molecular radial distributions.” In the other inserts of Figure 7, we report for the first five $^1\Pi_u$ states the “state- $D_{nl}(r)$ ” plots for the internuclear distances of 0.5 and 2.0 bohrs (middle insets) and 4.0 and 15.0 bohrs (bottom insets). The identification of the first five state- $D_{nl}(r)$ for $R = 0.5, 2.0, 4.0$, leads to $1(1s2p)$, $2(1s3p)$, $3(1s4f)$, $4(1s4p)$, and $5(1s5f)$, obtained by simple inspection of the united atom

TABLE III

$^1\Pi_g$ manifold: configurations $1snl$ for states 1 to 10 at different internuclear separations: nl from “state- $D_{nl}(r)$ ” analyses, (nl) from basis subset analysis (see text).

#	0.1	0.5	1.8	2.0	2.2	3.0	4.0	5.0	6.0	8.0	10.0	15.0	30.0	100
1	3d	3d	3d	3d	3d	3d	2p	2p	2p	2p	2p	2p	2p	2p
2	4d	4d	4d	4d	4d	4d	3p	3p	3p	3d	3d	3p	3p	3d
3	5d	5d	5d	5d	5d	5d	4p	4d	3d	3p	3p	3d	3d	3p
4	5g	4p	4d	4p	4f	4f	4f							
5	6d	6d	6d	6d	6d	6d	5p	5d	4d	4f	4f	4d	4d	4d
6	6g	6f	5p	4p	(4p/4d)	4p	4p	4p						
7	7d	7d	7d	7d	7d	7d	6d	6g	5f	5d	(5l)	5g	5g	5g
8	7g	7g	7g	7g	7g	7g	6p	6d	6p	(5d/5f)	(5d/5f)	5f	5f	5f
9	8d	8d	8d	8d	8d	8d	7g	7d	6d	(5l)	(5l)	5d	5d	5d
10	8g	8g	8g	8g	8g	8g	7d	7g	6g	5p	(5l)	5p	5p	5p

TABLE IV

³ Π_u manifold: configurations 1snl for states 1 to 10 at different internuclear separations: nl from “state-D_{R,nl}(r)” analysis, (\geq nl) from basis subset analyses.

#	0.1	0.5	1.8	2.0	2.2	3.0	4.0	5.0	6.0	8.0	10.	15.	30.	100
1	2p	2p	2p	2p	2p	2p								
2	3p	3d	3d	3d	3p	3d								
3	4p	4p	4p	4p	4p	4f	4f	4f	3d	3d	3p	3p	3d	3p
4	4f	4f	4f	4f	4f	4p	4p	4p	4p	4f	4f	4f	4f	4f
5	5p	5p	5p	5p	5p	5f	5f	5f	4d	4f	5g	4d	4d	4d
6	5f	5f	5f	5f	5f	5p	5p	5p	5p	4d	5g	5g	4p	4p
7	6p	5f	(\geq 5l)	4p	(\geq 5l)	5g	5g							
8	6f	6d	6p	(\geq 5l)	5f	(\geq 5l)	5f	5f						
9	6h	7l	6d	(\geq 5l)	(\geq 5l)	(\geq 5l)	5d	5d						
10	7p	7l	6f,6d	(\geq 5l)	(\geq 5l)	(\geq 5l)	5p	5p						

distributions. For $R = 15.0$ bohrs the five state-D_{nl}(r) distributions are obtained by inspection of the references D_{nl}(r) at $R = \infty$ and are 1s2p, 1s3d, 1s3p, 1s4f, and 1s4d. Below we use the shorthand notation nl in place of 1snl.

By inspection of the computed PECs (Figures 3 and 5), the region from about 6 to 10 bohrs is expected to be of difficult identification particularly for the states, which dissociate at $n = 5$.

Let us consider for example, the ¹ Π_u states in detail (see Table II). For state 1 we observe a “regular” evolution from the united atom to dissociation. Same for state 2, where we recall the near degeneracy of H[²P(3p¹)] and H[²D(3d¹)] energies at dissociation. For state 3, the united atom configuration survives till 5 bohrs (thus well beyond the equilibrium distance), then after a switch around 6 bohrs into 3d it slowly approaches the degenerate energies of states H[²P(3p¹)] and

H[²D(3d¹)], expected by inspection of the PEC of Figure 3. State 4 is a “regular” state, maintaining constantly configurations with $n = 4$. States 5 and 6 again retain the united atom configuration till about 5 bohr, then there is a switch from $n = 5$ to $n = 4$, with a rather fuzzy identification for state 6, which crosses state 7 at about 6 bohrs. States 7 and 8 are very close to each other from 7 to about 10 bohrs, and this is a region of high fuzziness. For states 9 and 10, the region of near degeneracy (8 to 10 bohrs) leads again to fuzziness.

For the ¹ Π_g manifold simple inspection of the PECs in Figure 3 leads to expect fuzziness in the neighborhood of 4 bohrs and again in the region between 6 and 10 bohrs because of state crossing and near-crossing. Table III confirms these expectations. For the states 1, 2, and 3 the united atom configuration “survives” till about 4 bohrs, a shorter distance relative to that in the ¹ Π_u states.

TABLE V

³ Π_g manifold: configurations 1snl for states 1 to 10 at different internuclear separations: nl from “state-D_{n,l}(r)” analysis, (\geq nl) from basis subset analyses.

#	0.1	0.5	1.8	2.0	2.2	3.0	4.0	5.0	6.0	8.0	10.	15.	30.	100
1	3d	2p	2p	2p	2p	2p	2p	2p						
2	4d	3d	3d	3d	3d	3d	3d	3d						
3	5d	4d	3p	3p	3p	3p	3p	3p						
4	5g	5d	4d	4f	4f	4f	4f	4f						
5	6d	5p	5g	4f	4d	4d	4d	4d						
6	6g	6f?	5d	(\geq 4l)	(\geq 4l)	(\geq 4l)	4p	4p						
7	7d	6p	6g	5g	5f	(\geq 5l)	5g	5g						
8	7g	7g	7g	7g	7g	7g	7d	6d	6d	(\geq 5l)	(\geq 5l)	(\geq 5l)	5f	5f
9	8d	8d	8d	8d	8d	8d	7g	7d	6p	5f	(\geq 5l)	(\geq 5l)	5d	5d
10	8g	8g	8g	8g	8g	8g	7p	7g	(\geq 5l)	(\geq 5l)	(\geq 5l)	(\geq 5l)	5p	5p

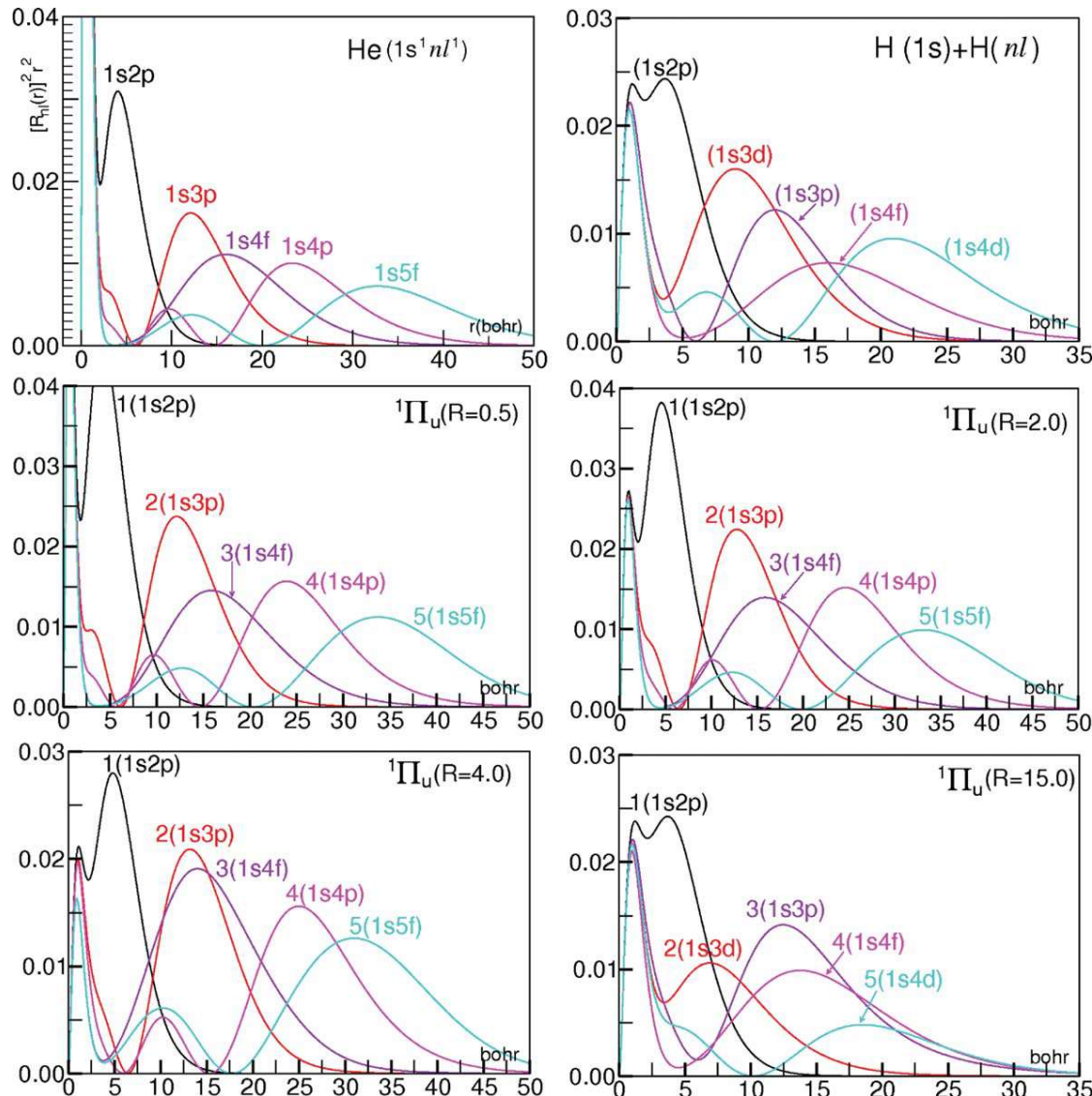


FIGURE 7. ${}^1\Pi_u$ states 1 to 5: molecular radial distribution “state- $D_n(r)$ ” at $R = 0$ and $R = \infty$ (top), at $R = 0.5$ and 2.0 bohrs (middle) at $R = 4.0$ and 15.0 bohrs (bottom). [Color figure can be viewed in the online issue, which is available at wileyonlinelibrary.com.]

Switches between configurations are noted for states 2 and 3 around 6 and 30 bohrs. The pairs of states 4 with 5, and 6 with 7 are nearly degenerate in the neighborhood of 5 bohrs, and this causes fuzziness. The states 7 and 8 are nearly degenerate in the region 6–10 bohrs; states 9 and 10 in the region 7–10 bohrs.

Our analysis nicely confirms findings by Wolniewicz [12] and Stephens and Dalgarno [50] on low states. From Stephens and Dalgarno perturbational computations the configurations for the second and third ${}^1\Pi_u$ states are $1s3d$ and $1s3p$ at dissociation,

respectively. Wolniewicz assigns the configurations of the second and third ${}^1\Pi_u$ states at $R = 15.0$ and 25.0 bohrs to $1s3d$ and $1s3p$, respectively; for the second and third ${}^1\Pi_g$ at $R = 15$ bohrs the configurations are $1s3d$, $1s3p$, and at $R = 25$ bohrs $1s3p$ and $1s3d$. From our data the above characterizations hold till about 30 bohrs, but at 100 bohrs the second and third ${}^1\Pi_g$ state configurations are switched to $1s3d$ and $1s3p$, respectively.

Tables IV and V allow to follow state by state the density evolution in the ${}^3\Pi_u$ and ${}^3\Pi_g$ manifolds.

For the four Δ manifolds inspection of the PECs in Figure 5 leads to expect fuzziness particularly in the interval 8 to 15 bohrs because of state crossing and near-crossing, concomitant with the lowering of the n value from united atom to dissociation. This is more evident in the $^1,^3\Delta_u$ relative to $^1,^3\Delta_g$ manifolds. State 1 of the $^1,^3\Delta_g$ maintains the $1s3d$ configuration from united atom to dissociation. State 2 at 15 bohrs switches from the configuration $1s4d$ of the united atom to the $1s4f$ configuration, which remains constant till dissociation. State 3 keeps the $1s5g$ united atom configuration till about 7 bohrs, where it switches to the configuration $1s4f$ and then at 15 bohrs to the $1s4d$ configuration. State 4 has $1s5d$ configuration at the united atom, at 7 bohrs is a mixed configuration $1s5l$, which becomes $1s5g$ at about 10 bohrs and remains constant till dissociation. State 5 starts as $1s6d$, at about 3 bohrs becomes $1s6g$, at 8 bohrs is $1s5d$, and from 15 bohrs to dissociation has configuration $1s5f$. State 6 starts as $1s6g$, becomes $1s6d$ at 3 bohrs, then around 7 bohrs it becomes a mixed configuration $1s6d/1s6g$, finally from 15 bohrs till dissociation is $1s5d$.

State 1 of the $^1,^3\Delta_u$ maintains the $1s4f$ configuration from the united atom to 5 bohrs, then becomes a mixed configuration $1s3d/1s4f$ and immediately after is a $1s3d$ configuration till dissociation. State 2 at 5 bohrs switches from the configuration $1s5f$ of the united atom to the $1s4f$ configuration, which remains constant till dissociation. State 3 keeps the $1s6h$ united atom configuration till about 5 bohrs, where it switches to the configuration $1s5f$ and then at 8 bohrs to the $1s4d$ configuration. States 4, 5, and 6 have at the united atom configuration $1s6f$, **1s7f** and $1s7h$, respectively which are maintained till 5 bohrs. From there to 10 bohrs have mixed configurations, the dissociation configurations are $1s5g$, $1s5f$, and $1s5d$.

Both the Φ_u and Φ_g manifolds are rather regular also in n -matching region. The three Φ_u states maintain the united atom configuration $1s4f$, $1s5f$, and $1s6h$ till about 12 bohrs, thereafter for states 2 and 3 there is a switch to $1s5g$ and $1s5f$, the dissociation configurations. The three Φ_g states maintain the united atom configuration $1s5g$, $1s6g$, and $1s7g$ till about 7 bohrs, thereafter there is a switch to $1s4f$, $1s5g$, and $1s5f$ the dissociation configurations. The Γ state has the same configuration, $1s5g$, from the united atom to dissociation.

All in all, the state- $D_n(r)$ analysis leads to a dynamic picture of density variations with R . This dynamics reflects the variations in the electron-

electron and nuclear-electron interactions, particularly notable at near state crossing, involving two or even more states. Because of these variable interactions the electron pair in a given PEC undergoes rapid delocalization over a small bond distance range and configuration mixing, which can lead to fuzziness in the electronic density.

The analysis clearly points out that an excited state in H_2 should not be considered as a state independent from the others, because the strong interactions propagate from state to state via mixed configurations; even the symmetry appears not to be a sufficient constraint to bring about clear energy differentiation between different manifolds.

7. Analysis with the Basis Subset Decomposition

In the second-type of analysis, designated "the basis subset decomposition", we recompute each PEC selecting appropriate subsets of the full basis set: in this way we determine those basis functions needed to correctly reproduce a selected PEC as given in Figures 1–6, namely obtained with the full set. As expected, relatively few subsets are needed to represent a specific PEC and, therefore, the subset decomposition approach leads to the identification of the prominent basis functions in a given state at a given internuclear separation. Again, for states strongly interacting or nearly crossing or crossing, several basis subsets are needed to represent the mixing of configurations. We exemplify in some detail this type of analysis for the states of the $^1\Pi_u$ manifold (see Table II).

For the $^1\Pi_u$ manifold the basis subset formed by all the s and p functions, denoted simply as nsnp, essentially reproduces states 1, 2, and 3 from the united atom to dissociation and partially state 8 from about 7.5 to 18 bohrs. In Figure 8, we report the potential energy curves obtained from four basis subsets, specifically nsnp, nsnp3d4d, nsnp3d4d4f, and nsnpnd4f; we focus only on the high excited states and in the internuclear distance region between 6 to 12 bohrs, a region insufficiently characterized by the molecular probability distribution analysis. We use colors to differentiate curves from different subsets: the black color (full line) for the full basis set computations, violet color (dotted line) for the subsets nsnp, green color (dashed line) for nsnp3d4d, magenta color (dotted line) for nsnp3d4d4f, and red color

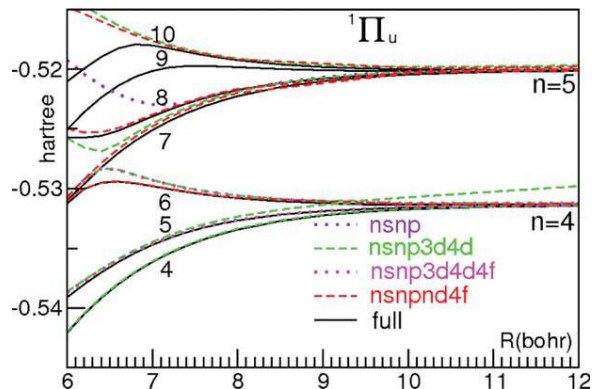


FIGURE 8. Examples of basis subset analysis for high excited $^1\Pi_u$ states. [Color figure can be viewed in the online issue, which is available at wileyonlinelibrary.com.]

(dashed line) for nsnpnd4f. State 4 is essentially reproduced by the nsnp3d4d subset, state 5 by the nsnp3d4d4f subset; information already available from the previous analysis and now reconfirmed. State 6 was not clearly characterized between 8 and 10 bohrs; it needs nsnpnd4f, and therefore, the characterization (4l/5d) is given in Table II. State 7 is not characterized in the region 8–15 bohrs, but from Figure 8 we see that it needs nsnpnd4f subset, thus it can be characterized by the mixed configurations 4l and 5d, therefore the notation (4l/5d) is given in Table II. State 8 is not characterized in the region 8–10 bohrs, the nsnp subset reproduces the PEC from 9 bohrs to large distances, however at shorter internuclear distances the nsnpnd4f subset is important, thus we give the characterization (5p/5d) in Table II. State 9 is not reproduced with subsets, it needs the full set, thus the characterization is (5f/5g). State 10 from 8 to 15 bohrs needs a better characterization. From the subset analysis there is mixing of configurations, particularly 4l/5l.

Our analysis on the 140 states (see Refs. [1–3] for the Σ states) shows that the states are generally described by a dominant configuration $1s_{nl}$, with n at the united atom equal or different from that at dissociation, n' . In general, for low energy states $n = n'$. For high energy states $n > n'$. The analysis shows that the PECs can be partitioned into three contiguous internuclear distance regions. The first region starts at the united atom and ends beyond the equilibrium distance, here $n = n'$. The second region starts at the dissociation products, with configurations $1s + n'l'$, and ends around 10–20 bohrs maintaining the same n' value. The third region is

intermediate between the previous two; in this region there is the matching of the principal quantum number n of the He configuration $1s_{nl}$ with the dissociation product configuration $1s$ and $n'l'$ of the H atoms. We call this the “ n -matching region”. The matching for $n \neq n'$ occurs mainly via state crossing, and energetically produces “irregularities” in the PECs. For states with dissociation products $1s + nl$ with $n = 1, 2$, and 3 the PECs do not exhibit the n -matching region, and are rather smooth functions of the internuclear distances. For states dissociating with $1s + nl$ where $n = 4$ and 5 the PECs display irregularities in the n -matching region; thus a full representation of the H_2 molecule demands consideration of high excited states.

The n -matching region is expected to be more relevant for manifolds of low Λ value (thus with many states below the H_2 molecular ion) and, for a given manifold, is more extended the higher the state. Indeed, the difference $\Delta n = n - n'$ (at united atom and at dissociation) is $8 - 5 = 3$ for the highest state of the Σ and Π manifolds, and $6 - 5 = 1$ for the Δ and Φ (see also Table I). Thus, not only we can predict with computations the existence of the irregularities in the PECs but also differentiate the irregularity relevance manifold by manifold and, within a given manifold, low from high states.

8. Hund’s Multiplicity Rule

The excited states belong to symmetry manifolds characterized by quantum constraints, $\Lambda = \Lambda m_{L1} + m_{L2}$ | the absolute value of the component of orbital angular momentum along the internuclear axis, inversion symmetry, gerade or un-gerade, and spin multiplicity ($2S + 1$).

Empirical evidences on line spectra have as long ago lead to rules on the energy stability relating states of different multiplicity. The semi-empirical Hund’s multiplicity rule [51] asserts that the state of highest multiplicity is the most stable, “other things being equal” [52]. The relative “extra” stability has been related to differences in the electron–electron repulsion [53] and concomitant electronic density interaction with the nuclear charges. This effect is expected to hold in systems both with or without nuclei, as recently pointed out for two-electron quantum dots [54]. In the following, we consider the triplet-singlet splitting as obtained from our computations, including also those of Σ manifolds [1–3].

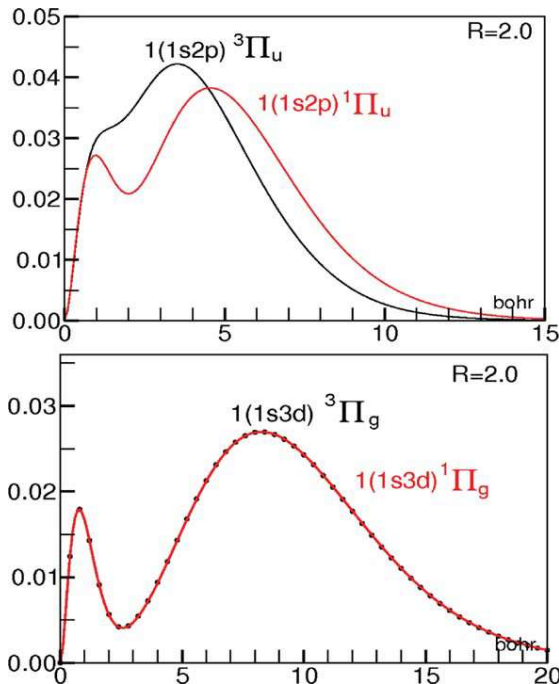


FIGURE 9. Hund's multiplicity rule. Radial distribution functions for the lowest Π states at 2.0 bohrs. [Color figure can be viewed in the online issue, which is available at wileyonlinelibrary.com.]

The Hund's splitting is large for the first two states of Σ and Π_u manifolds and decreases notably for higher states; at the equilibrium distance, for the first two excited states the $^3,1\Sigma_g$ splitting (in hartree) is -0.0180 and -0.0001 , respectively; and for the $^3,1\Sigma_u$ is -0.1814 and -0.0177 , respectively. The $^3,1\Pi_u$ splitting is -0.0193 and -0.0054 and there is essentially no splitting for the $^3,1\Pi_g$ states. The above largely different splitting can be explained by considering the different electronic configurations, for example for the first states $^3,1\Pi_u$ and $^3,1\Pi_g$. In Figure 9 we plot for the internuclear distance 2.0 bohrs the molecular probability distribution functions for the first state of $^3\Pi_u$ and $^1\Pi_u$, and of $^3\Pi_g$ and $^1\Pi_g$ symmetries. In the top inset we see that the 1s and the 2p electrons in the $^3\Pi_u$ state are nearer to each other than in the $^1\Pi_u$ state, thus with larger electron-electron repulsion, and concomitant larger nuclear-electron attraction. However, this is no longer the case for the $^3\Pi_g$ compared with the $^1\Pi_g$ (bottom inset), where the two electrons have very similar probability distributions in the two states, leading to a splitting of -5×10^{-4} hartree. We could

argue that the large difference in the electronic density is also related to a change in the quantum numbers nl .

We have considered—in addition—the total energy components for the Σ and Π manifolds. Figure 10 reports the nuclear-electron, n-e, the kinetic, k , and the electron-electron, e-e, energy components versus the internuclear separation for the first two states of the Σ (top insets) and of the Π (bottom inset) manifolds. At equilibrium distance the three energy components clearly show near degeneracy for the first $^1\Pi_g$ and $^3\Pi_g$ states. In the Σ and Π_u manifolds the energy components of the triplet states are larger than those of the singlet, with the electron-nuclear attraction larger (more attractive) than the sum of the electron-electron and kinetic energy components. Thus, as expected the Hund's rule is verified.

We consider now the splitting for the Δ , Φ , and Γ states. The computed PECs show strong degeneracy for the $^1\Delta_g$ with the $^3\Delta_g$ states and for the $^1\Delta_u$ with the $^3\Delta_u$ states. This holds also for the Φ and Γ manifolds. Quantitatively the first Δ_g state presents a splitting of -6×10^{-5} hartree, and there is essentially no-splitting between the $^1\Delta_u$ and $^3\Delta_u$ states.

An observation is added: The splitting above analyzed can be considered as “propagation” from the He atomic triplet-singlet splitting to the molecular system. For example, from the Moore's tables [48] we obtain that in the He atom the triplet-singlet splitting for P states with configurations 1s2p and 1s3p is -9.3229 and -2.9297 mhartree, respectively. Equivalently, the He triplet-singlet splitting in the D states with configurations 1s3d and 1s4d is -0.0107 and 0.0025 mhartree, respectively. These values and trends are comparable with those here reported for the H₂ molecule.

9. Correlation Energy and Total Energy Decomposition

The availability of full CI energies allows a short detour on the correlation energy correction and on the reasons for the stability (atomization energy) of the electronic states.

In this work, the correlation energy is defined as the energy difference between the exact non relativistic energy and the energy from a specified model $E_c(\text{model})$ [55]. Much of today literature follows a definition proposed by Löwdin [56] which—

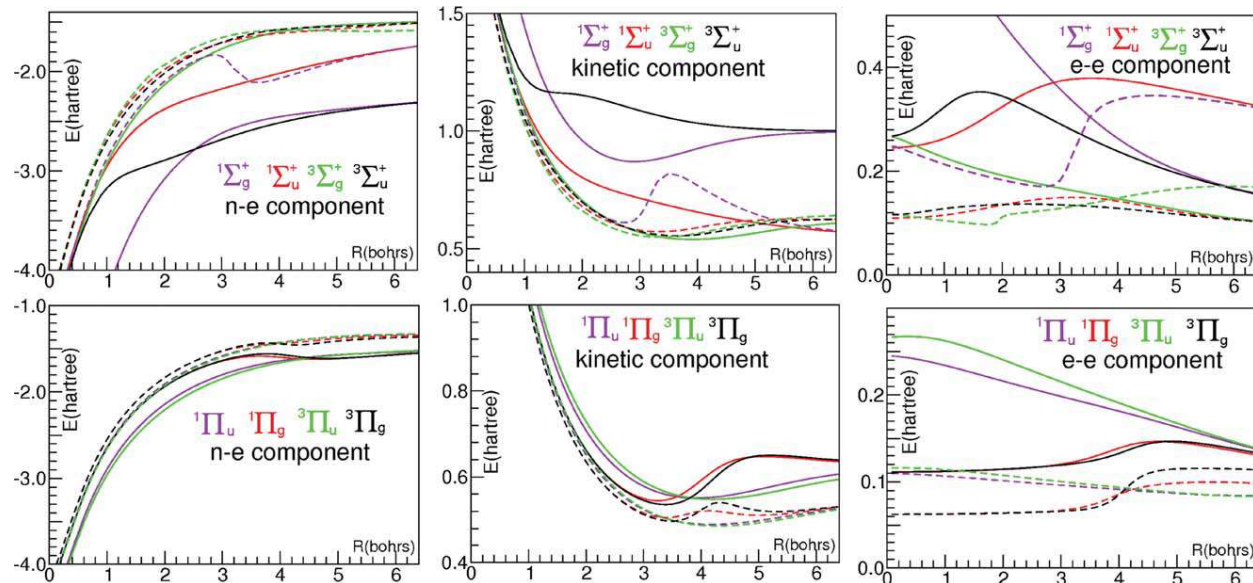


FIGURE 10. Energy components for the first (full lines) and second (dashed lines) in the $^1\Sigma_g^+$, $^1\Sigma_u^+$, $^3\Sigma_u^+$, $^3\Sigma_g^+$ states (insets in first rows) and in the $^1\Pi_u$, $^3\Pi_u$, $^1\Pi_g$, $^3\Pi_g$ states (insets in second row). [Color figure can be viewed in the online issue, which is available at wileyonlinelibrary.com.]

somewhat arbitrarily in our opinion—considers the Hartree–Fock approach as the reference model in the definition of the correlation energy. As we use two models, the Hartree–Fock and the Heitler–London, we distinguish two different correlation corrections, $E_c(\text{HF})$ and $E_c(\text{HL})$. In H_2 the $E_c(\text{HL})$ correlation correction, being zero at dissociation, fully and directly relates to the atomization energy; as we all know this is not the case for $E_c(\text{HF})$. In Table VI we report and compare $E_c(\text{HF})$ and $E_c(\text{HL})$ for the equilibrium distances of the three bound Σ lowest states; the trend in the $E_c(\text{HL})$ data is physically reasonable, not so for the $E_c(\text{HF})$, as noted in Ref. [55].

The correlation energy is a small fraction of the total energy; its importance is because of the realization that it can be a notable percentage of the molecular atomization energy. Clearly, when two electrons are far one from the other the electron–electron interaction is small and—a fortiori—the correlation correction becomes even smaller (this obvious consideration is fulfilled by $E_c(\text{HL})$ but not by $E_c(\text{HF})$). Therefore, we expect that the correlation energy will become smaller and smaller the higher the electronic excitation in the H_2 system as shown in Table VI.

The data in Table VI show that the $E_c(\text{HF})$ is not as essential—as sometimes assumed—for explaining the energy and internuclear distance

differentiation of the lowest states. The novel aspect highlighted by the table is that the $E_c(\text{HL})$ is very different from $E_c(\text{HF})$ and decreases notably fast with the internuclear distances.

At $R = 2.0$ bohrs the $E_c(\text{HF})$ values (in mhartree) for the lowest $^1\Pi_g$ and $^1\Pi_u$ states are -0.921 , -4.225 , and for the $^3\Pi_g$ and $^3\Pi_u$ states -0.653 and -4.486 , respectively. For the $^1\Delta_g$, $^1\Delta_u$, $^3\Delta_g$, and $^3\Delta_u$ states the correlation effect, at $R = 2.0$ bohrs, is smaller, -0.399 , -0.070 , -0.309 , and -0.070 mhartree, respectively; for the $^1\Phi_g$, $^1\Phi_u$, $^3\Phi_g$, and $^3\Phi_u$ even smaller, -0.117 , -0.099 , -0.117 , and -0.099 mhartree, respectively; negligible for the Γ states.

TABLE VI
“Traditional” Correlation Energy $E_c(\text{HF})$ in hartree at different internuclear distances (in bohrs).

R	$^1\Sigma_g^+$	$^1\Sigma_u^+$	$^3\Sigma_g^+$	$^3\Sigma_u^+$
1.40	-0.0406^{a}	-0.0059	-0.0018	-0.0057
1.90	-0.0450^{b}	-0.0102	-0.0022^{e}	-0.0045
2.40	-0.0529^{c}	-0.0155^{d}	-0.0029	-0.0031^{f}

$E_c(\text{HL})$: ^a -0.0235 , ^b -0.0193 , ^c -0.0152 , ^d -0.0107 , ^e -0.0011 , ^f -0.0023 .

Considering the HL model, the $E_c(HL)$ at $R = 2.0$ bohrs for the lowest $^1\Pi_u$ state is -2.426 mhartree and for the $^3\Pi_u$ state -3.523 ; for the $^1\Delta_g$ the value is -0.575 mhartree, and -0.502 for $^3\Delta_g$. These values become notably smaller at larger distances, as physically reasonable, contrary to the $E_c(HF)$ trend.

10. Covalent Binding

Concerning the atomization energy and the so called “origin of the covalent bond” we recall [4, 57] that (1) states with configurations of bonding orbitals (like $1\sigma_g^2$) have equilibrium at shorter distance and larger atomization energy than those of antibonding orbitals (like $1\sigma_g^11\sigma_u^1$), (2) the triplet states follow Hund’s empirical rule, (3) the orbital energies with increasing equilibrium internuclear separation are in the order $1\sigma_g > 2\sigma_g > 1\pi_u\dots$, (4) because of Pauli principle the first $^3\Sigma_g^+$ state has configuration $1\sigma_g2\sigma_g$, and (5) the bond energy changes with the distances, and fullfills the virial theorem (stating that the average kinetic energy, T , and potential energy, V , are $T = -E - R(\delta E/\delta R)$ and $V = 2E + R(\delta E/\delta R)$ for two nuclei at distance R in a system with energy E).

Analyses of the covalent binding energy are available—since long ago—in quantum chemistry textbooks, for example [52, 58]. The above generic and qualitative comments on binding lead to the expectation that the $^1\Sigma_g^+$ ground state, $1\sigma_g^2$, is the state with the lowest energy and with shorter internuclear separation relative to the corresponding $^1\Sigma_u^+$ state (with an antibonding orbital in the configuration $1\sigma_g^11\sigma_u^1$, which shifts the minimum to larger distances). The $^3\Sigma_g^+$, $1\sigma_g^12\sigma_g^1$, is expected to be less binding and at a larger equilibrium distance than the $^1\Sigma_g^+$ because of the promotion of one electron from $1\sigma_g$ to a $2\sigma_g$ orbital. The $^3\Sigma_u^+$ is expected to be at a lower energy than the $^1\Sigma_u^+$ (Hund’s rule). The second $^1\Sigma_g^+$ state (the EF state) with configuration $1\sigma_g^12\sigma_g^1$ is expected to have a minimum at about the same distance as the first $^3\Sigma_g^+$ state, with the triplet state at a lower energy (Hund’s rule). In this qualitative analysis, following tradition, the eventual contribution from ionic energy components is ignored.

These qualitative reasoning can be confirmed by a more quantitative analysis presented in previous computations [1–3], by the energy data of this work and by decomposing the total energy into its com-

ponents $E(k)$, $E(n-e)$, and $E(e-e)$. Note that a simple inspection of the 140 states energies (Figs. 1–6) clearly points out the importance of the u , g classification and the fast departure from the Hund’s multiplicity empirical rule following an increase of the principal quantum number at the united atom.

In Figure 11 we consider, as examples, a few states out of the 140 computed, specifically the first and second states of the Σ symmetries, analyzed in the top two rows of insets and the lowest state of Π symmetries analyzed in the bottom insets. In this figure we “build-up” the binding energy using of the total energy components reported in Figure 10.

The total energies of the 140 states have in common the same nuclear–nuclear repulsion curve, $E(n-n)$, which from zero value at dissociation increases to very high values in approaching the united atom, but suddenly drops to zero at the united atom (due to the fusion of the two nuclei). Clearly the correct binding for a given state is obtained by considering each one of the total energy components, which are not independent quantities, since constrained by the virial theorem.

In the Figure 11 for all the states considered the $E(n-e)$ attraction is the lowest curve (in violet color). Note that the energy scale of Figure 11 is much larger than needed for the H_2 total binding energies, which are only a fraction of some of the energy components. The energy sum $E_2 = [E(n-n) + E(n-e)]$ (curves in red color) are characterized by a well developed energy minimum, from very deep to relatively shallow (compare, for example, the first $^1\Sigma_g^+$ state with the first $^3\Sigma_u^+$ state). This minimum is expected, since in H_2 the four nuclear-electron attraction terms yield an attractive interaction larger than the $E(n-n)$ repulsion. Addition of the $E(e-e)$ repulsion leads to the energy $[E(n-n) + E(n-e) + E(e-e)]$ curves (green color), which all show the persistence of the energy minima, now clearly less deep than for $[E(n-n) + E(n-e)]$. Note that the $E(e-e)$ curve for the singlet states are expected to differ from those of the triplet states because of the exchange energy contribution.

The systems considered are all subjected to the virial theorem, for which at equilibrium $T = -E$ and $V = 2E$. The computed $E(k)$ value added to $[E(n-n) + E(n-e) + E(e-e)]$ leads to the total energy (curve in black color), thus to the binding (atomization) energy, obtained by subtraction of the dissociation energy value. The $E(k)$ contribution

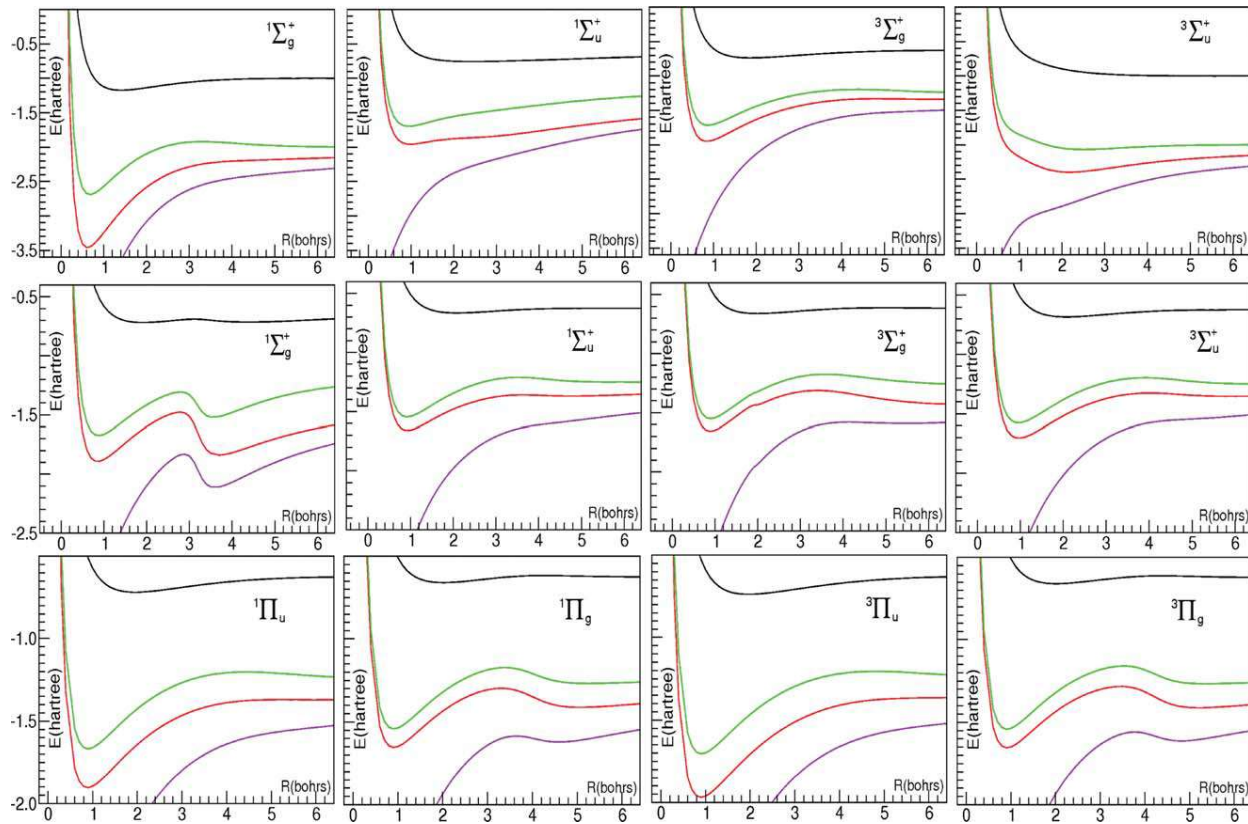


FIGURE 11. Total binding energy build up (black curves) for the first and second states in the Σ manifolds (insets in top two rows) for the lowest Π states (insets in third row): $E_1 = E(n-e)$ in violet, $E_2 = E_1 + E(n-n)$ in red, $E_3 = E_2 + E(e-e)$ in green, $E_4 = E_3 + E(K)$ in black. [Color figure can be viewed in the online issue, which is available at wileyonlinelibrary.com.]

appears to be responsible for the position of the energy minima.

Note that the $E(n-e)$ curves notably differ state by state and characterize the entire process leading to the final binding energy values; however, the other energy components are also all necessary to yield the final binding. Thus, the origin of binding is seen as the global response to the evolution of the molecular electronic density, which, as we know, varies with the internuclear separation state to state.

In conclusion, we have presented an idealized build-up process rationalizing the formation of covalent binding both for the ground and for the excited states. Recall that mention to the virial is tantamount to mention the kinetic energy, often assumed to be the “origin” for binding in homopolar molecules [58–60]. Note that this traditional type of analysis ignores alternative explanation

offered for example by the Hellmann–Feynman theorem.

11. Comment on the Adiabatic Correction

The regions where the adiabatic correction is expected to be relevant are mainly at state crossing, clearly available from the B-O PECs computations. In Figure 12, we present our PECs for a few $^1\Sigma_u$ states (solid black lines) compared with selected values from Wolniewicz computations [16]: black circles and red bullets for computations without and with adiabatic correction, respectively. The adiabatic correction is relatively small; as expected it increases significantly at crossing of states. In Figure 12, we see a crossing (full black line)

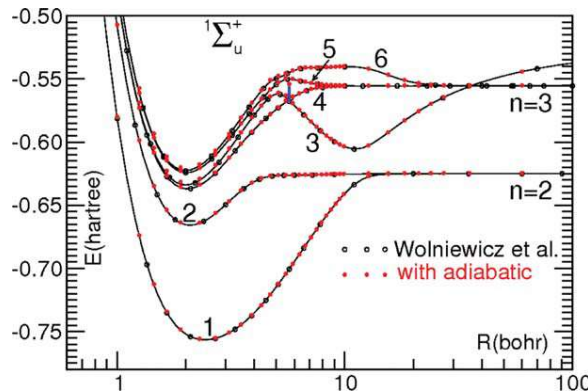


FIGURE 12. The first six $^1\Sigma_u^+$ states: Full-CI B-O computations (full lines), computations from Ref. [58] with and without adiabatic corrections, red bullets and open circles, respectively. [Color figure can be viewed in the online issue, which is available at wileyonlinelibrary.com.]

between the states 3 and 4 at about 5.9 bohrs, where we expect a large adiabatic correction (red circles), as indeed computed [16], represented in the figure with the vertical blue bar: note that this correction is a local sudden peak. As apparent from the figure, most of the PECs with adiabatic correction have energy very near to our B-O data, being the adiabatic correction generally small. Computationally, it is a straight ford, but computer expensive, task to obtain the adiabatic correction; availability of accurate total energies from B-O computations is the main requirement for computing the adiabatic correction if one uses numerical energy differences [61].

The B-O PECs can be used as a first approximation to computationally obtain vibrational constants, clearly in need of eventual adiabatic corrections, when these become significant. For example, computed spectroscopic constants obtained from the B-O PECs for the first two $^1\Pi_u$ states yield $\omega_e = 2446.94$ and 2360.27 , respectively, $\omega_{ex}e = 70.04$ and 68.22 , $\beta_e = 30.58$ and 29.61 , $R_e = 1.9519$ and 1.9831 bohrs, in good agreement with the experimental values given in Ref. [43]. Work is in progress (Corongiu and Clementi, unpublished data) to systematically compute the B-O spectroscopic constants for the 140 states.

The obvious suggestion front the above comparison is that to obtain reasonable spectroscopic constants the first priority is to have good B-O PECs, the second is to add adiabatic corrections if and where the adiabatic correction is large, namely in the neighbor-

hood of state crossing or when two states are very close in energy (both conditions easily seen by inspection of accurately computed B-O PECs).

12. Conclusions

This study concludes the full CI computations, in the B-O approximation, of the PECs for the ground and excited states for the H_2 molecule. We have adopted the full CI technique, a well tested approximation, using both extended STF and spherical GTF basis sets, namely basis sets currently used in computational chemistry. Our computed energies are reliable as demonstrated by the excellent agreement with the best available in literature, the difference at the equilibrium separation varies from 2×10^{-6} up to 8×10^{-5} hartree.

The now available PECs of the lowest 140 states are obtained systematically using the same approximation, the same basis set, and are complemented with a uniform density analysis. The computations start at the united atom and extend from 0.01 bohrs to full dissociation. We predict PECs for the high excited states, previously unexplored, and provide a detailed state-by-state analysis, evidencing the electronic density evolution from the united atom to dissociation and the regions where one configuration is dominant, where multiconfigurations and where adiabatic correction are needed.

The approach of the PECs to the united atom energy (He isotope with mass 2) is consistently smooth, as previously found for the Σ manifolds [1–3]. The PECs of the Π states are somewhat more regular relative to those of the Σ states, partly due, for a given manifold, to the lower number of states crowding the energy interval between the first excited state and the H_2^+ ground state; this trend continues, considering the Δ , Φ , and Γ manifolds, with the Hund's splitting gradually reducing to zero.

The use of HL-CI has allows to asses ionic structures; we have found that the ionic character for the Π states is notably small, and negligible for the Δ , Φ , and Γ manifolds, differently from the finding in a few states of the Σ manifolds [1–3], where the ionic contribution is very relevant. The quantitative assessment of the ionic component, essential to understand the low electronic states in the Σ states, has been often neglected from theoretical considerations.

The united atom configuration for the Σ , Π , Δ , Φ , and Γ states is predominant not only at very short internuclear separations, as fully expected, but it extends into regions well beyond the equilibrium internuclear distance. Note that for the lowest Σ states the $1snl$ configuration at united atom changes into $1sn'l'$ at equilibrium, thus maintaining the same n value (exception made for the $^3\Sigma_u$ where the united atom $1s2p$ goes into $H_2(1\sigma_g1\sigma_u)$ the latter essentially built with $1s$ orbitals). Neither one of the two basic traditional theoretical approaches, molecular orbitals (and Hartree–Fock) and Heitler–London (and Valence Bond) have sufficiently recognized the “survival” of the united atom configuration at large distances, despite the clear acknowledgment [4, 57] that the molecular formation process starts at the united atom. For high excited states starting at the united atom and proceeding to dissociation—the electronic configurations evolve from $1snl$ to $1sn'l'$ with n larger than n' .

These observations suggest to consider a complementary proposal concerning the formation of H_2 in excited states. Since the early 1930s [4, 57] the standard assumption is that, starting from a helium atom two hydrogen atoms can be generated, with intermediate formation of the H_2 molecule. Computationally this process can be simulated either with full HF-CI or with full HL-CI (both techniques, unfortunately, requiring a large number of determinants, for example, $\sim 10,000$ determinants are needed in the H_2 computations reported in this work) or with different techniques.

The data from our study can be rationalized with an alternative mechanism where the starting assumption is the availability of a state of the molecular ion, H_2^+ to which one electron in a new orbital is added. Differently stated, the H_2^+ system in a state with configuration nl captures a second electron which assumes configuration $n'l' = ls$ at the united atom and at dissociation. This process can be viewed as an incoming electron “adapting” itself to the H_2^+ system, with an electron-electron repulsion as small as possible (thus with an average electron-electron distance as large as possible). Near equilibrium distances, for high nl quantum numbers, the interaction of this second electron with the first is relatively small, but it increases by decreasing the value of n ; for n larger than 2 the equilibrium distance of H_2^+ is retained (-2.0 bohrs) for the newly generated H_2 system. The two electrons are clearly distinct and different.

From Tables II to V as well in Refs. [1–3] we have followed the adaptation process of the second electron. For states with high n values at dissociation the two electrons are far from each other, even for relatively short internuclear distances (see Fig. 7, bottom left inset, where, for example, at the internuclear separation of 2 bohrs the 5f molecular probability distribution peak is ~ 35 bohrs far from the 1s peak, which is at 1 bohrs). For states with low n values at dissociation the electronic density peak of 1s and nl are relatively nearer (with concomitant strong interactions) and finally for the ground state the two probability peaks coincide. This evolution of the electronic density, however, does not imply that one has to adopt the MO approach, which accommodates both electrons in one molecular orbital. We recall Slater analysis [62] on nonorthogonal atomic orbitals, with the interesting conclusion that the Heitler–London approach is superior to the MO approach definitively for H_2 , and, likely, in general for any molecular system. In a relatively recent proposal, named the Hartree–Fock–Heitler–London approach [63, 64], we have computationally shown in a systematic study of diatomic molecules the value of Slater suggestion. Further from the present study, most naturally, the H_2 excited states are represented by “different orbitals for different spins”, a concept which has been extended to molecules since long ago [56]. Note that the suggestions of “nonorthogonality” and “different orbitals for different spins” [65–67] are part of the Hartree–Fock–Heitler–London approach [63, 64].

Recently, we have included in the one-electron orbital representation an explicit contribution from the united atom configuration, leading to a new type of nonorthogonal one-electron function, designated “chemical orbital” [68, 69]. The new representation yields accurate binding with less than one dozen determinants and by construction it yields correct dissociation products. The chemical orbital one-electron function is constructed with three functions, one particularly adapted to represent the united atom, one for the intermediate internuclear region and the third for dissociation. The present excited states study with the “revelation” of three internuclear regions corroborates our proposal.

The PEC patterns of the 140 states of H_2 , despite the individual characterization including eventual strong irregularities in the n -matching region, seem to be easily explained provided one recognizes the paramount importance of the propagation and evolution of the electronic structure manifested by the evolution of the principal quantum number n (a) at the united atom, (b) in the n -matching region, and

(c) at dissociation. Note that the existence of the three contiguous regions has become evident by carrying out accurate computations from very short internuclear separations and of high excited states, as we have done in this article.

The chemical orbital approach [68, 69] appears to be a reasonable way to account for the three internuclear regions, however it remains a representation constrained with the B-O approximation. Indeed, the PEC crossings call for adiabatic corrections. On the other hand, the evolution of the electronic density from united atom to dissociation remains the main chemical feature of general interest, and it calls for a time dependent representation (keeping in mind concepts proposed in Refs. [29–33, 56, 65–69]).

We add a final sobering conclusion: the H_2 computations of all the excited states below H_2^+ , from very short internuclear separations to full dissociation and the analysis on the electronic density presented in this work have filled—but only in the B-O approximation—a gap in our knowledge for this most simple molecule, ...but, after about 1 century from Bohr's nearly exact determination of ground and excited state energies for the H atom.

References

1. Corongiu, G.; Clementi, E. *J Chem Phys* 2009, 131, 034301.
2. Corongiu, G.; Clementi, E. *J Phys Chem* 2009, 113, 14791.
3. Corongiu, G.; Clementi, E. *J Chem Phys* 2009, 131, 184306.
4. Herzberg, G. *Molecular Spectra and Molecular Structure. I. Spectra of Diatomic Molecules*; D. Van Nostrand Company, Inc.: Toronto, 1950.
5. Mulliken, R. S. *J Am Chem Soc* 1966, 88, 1849.
6. Mulliken, R. S. *Phys Rev* 1928, 32, 186.
7. Mulliken, R. S. *J Am Chem Soc* 1966, 88, 1849.
8. Mulliken, R. S. *Phys Rev* 1960, 120, 1674.
9. Kolos, W.; Wolniewicz, L. *J Chem Phys* 1965, 43, 2429.
10. Rychlewski, J. *J Mol Spectrosc* 1991, 149, 125.
11. Wolniewicz, L. *J Mol Spectrosc* 1995, 169, 329.
12. Wolniewicz, L. *J Mol Spectrosc* 1996, 180, 398.
13. Wolniewicz, L.; Dressler, K. *J Chem Phys* 1994, 100, 444.
14. Wolniewicz, L. *Chem Phys Lett* 1995, 233, 644.
15. Wolniewicz, L.; Staszewska, G. *J Mol Spectrosc* 2003, 220, 45.
16. Staszewska, G.; Wolniewicz, L. *J Mol Spectrosc* 1999, 198, 416.
17. Staszewska, G. *J Phys Chem A* 2001, 105, 2308.
18. Kolos, W.; Rychlewski, J. *J Mol Spectrosc* 1977, 66, 428.
19. Wolniewicz, L. *J Mol Spectrosc* 1995, 169, 329.
20. Wolniewicz, L. *J Mol Spectrosc* 1995, 174, 132.
21. Kolos, W. *J Chem Phys* 1994, 101, 1330.
22. Wolniewicz, L. *J Chem Phys* 1993, 99, 1851.
23. Wolniewicz, L.; Dressler, K. *J Chem Phys* 1994, 100, 444.
24. Wolniewicz, L. *J Chem Phys* 1998, 108, 1499.
25. Staszewska, G.; Wolniewicz, L. *J Mol Spectrosc* 2002, 212, 208.
26. de Lange, A.; Hogervorst, W.; Ubachs, W.; Wolniewicz, L. *Phys Rev Lett* 2001, 86, 2988.
27. Kolos, W.; Rychlewski, J. *J Mol Spectrosc* 1996, 177, 146.
28. Stenrup, M.; Larson, A.; Elander, N. *Phys Rev A* 2009, 79, 012713.
29. Deumens, E.; Diz, A.; Longo, R.; Öhrn, Y. *Rev Mod Phys* 1994, 66, 917.
30. Cabrera-Trujillo, R.; Sabin, J.R.; Öhrn, Y.; Deumens, E. *Phys Rev A* 2000, 61, 032719.
31. Killin, B. J.; Cabrera-Trujillo, R.; Deumens, E.; Öhrn, Y. *J Phys B* 2004, 37, 4773.
32. Hijikata, Y.; Nakashima, H.; Nakatsuji, H. *J Chem Phys* 2009, 130, 024102.
33. Nakatsuji, H.; Nakashima, H. *Int J Quant Chem* 2009, 10, 2248.
34. Heitler, W.; London, F. *Z Phys* 1927, 44, 455.
35. McLean, A. D.; Weis, A. W.; Yoshimine, M. *Rev Mod Phys* 1960, 32, 211.
36. James, H. M.; Coolidge, H. A. *J Chem Phys* 1933, 1, 825.
37. James, H. M.; Coolidge, H. A.; Present, R. D. *J Chem Phys* 1936, 4, 193.
38. Zemke, W. P.; Lykos, P. G.; Wahl, A. C. *J Chem Phys* 1969, 51, 5635.
39. Langhoff, S. R.; Huo, W. M.; Partridge, H.; Bauschlicher, C. W. *J Chem Phys* 1982, 77, 2498.
40. Detmer, T.; Schmelcher, P.; Cederbaum, L. S. *J Chem Phys* 1998, 109, 9694.
41. Spielfiedel, A. *J Mol Spectrosc* 2003, 217, 162.
42. Corongiu, G. *J Phys Chem* 2007, 111, 13611.
43. Huber, K. P.; Herzberg, G. *Molecular Spectra and Molecular Structure IV. Constants of Diatomic Molecules*; Van Nostrand Reinhold: New York, 1979.
44. Ishikawa, A.; Nakashima, H.; Nakatsuji, H. *J Chem Phys* 2008, 128, 124103.
45. Scherr, C. W.; Knight, R. E. *Rev Mod Phys* 1963, 35, 436.
46. Slater, J. C. *Phys Rev* 1930, 36, 57.
47. Clementi, E.; Raimondi, D. L. *J Chem Phys* 1963, 38, 2686.
48. Moore, C. E. *Atomic Energy Levels, NBS Circular 467 Vol. 1*; U.S. Government Printing Office: Washington, DC, 1971.
49. Pauling, L.; Wilson, E. B. *Introduction to Quantum Mechanics*; McGraw-Hill, Book Company: New York, 1935.
50. Stephens, T. L.; Dalgarno, A. *Mol Phys* 1974, 28, 1049.
51. Hund, F. *Linienspektren und periodisches System der Elemente*; Springer: Berlin, 1927; p 124.
52. Kauzmann, W. *Quantum Chemistry*; Academic Press: New York, 1957.
53. Slater, J. C. *Phys Rev* 1929, 34, 1293.
54. Sako, T.; Paldus J.; Diercksen, G.H.F. *Phys Rev A* 2010, 81, 022501.

55. Clementi, E; Corongiu, G. *Theochem* 2009, 123, 209.
56. Löwdin, P.-O. *Phys Rev* 1955, 97, 1474.
57. Selected Papers of Mulliken, R. S.; Ramsay, D. A.; Hinze, J., Eds.; The University of Chicago Press: Chicago, 1975.
58. Levine, I. N. *Quantum Chemistry*. Allyn and Bacon Inc.: Boston, 1970.
59. Feinberg, M. J.; Ruedenberg, K. *J Chem Phys* 1971, 54, 1495.
60. Goddard, W. A.; Wilson, C. W. *Theor Chem Acta* 1972, 26, 195.
61. Valeev, E. F.; Sherrill, C. D. *J Chem Phys* 2003, 118, 3921.
62. Slater, J. C. *J Chem Phys* 1951, 19, 220.
63. Corongiu, G; Clementi, E. *J Phys Chem A* 2007, 111, 5333.
64. Corongiu, G; Clementi, E. *J Phys Chem A* 2007, 111, 13611.
65. Linderbeg, J.; Öhrn, Y. *Propagators in Quantum Chemistry*; Academic Press: New York, 1973.
66. Ortiz, J. V. *Advances in Quantum Chemistry*. Academic Press: New York, 1999; Vol. 35.
67. Pauncz, R. *Different Orbitals for Different Spins, Löwdin's Idea. Fundamental Work of Quantum Chemistry*; Brändas, E. J., Kryachko, E. S., Eds.; Kluwer Academic: Boston, 2003; Vol. I, p 155.
68. Corongiu, G.; Clementi, E. *Am Inst Phys Conf Proc* 2009, 1102, 3.
69. Clementi, E.; Corongiu, G. *Int J Quant Chem* 2008, 108, 1758.